8891
NACA TN 2504

TECH LIBRARY KAFB, NM
0065506

NATIONAL ADVISORY COMMITTEE FOR AERONAUTICS

TECHNICAL NOTE 2504

EFFECTS OF WING POSITION AND HORIZONTAL-TAIL POSITION ON THE STATIC STABILITY CHARACTERISTICS OF MODELS WITH UNSWEPT AND 45° SWEPTBACK SURFACES WITH SOME REFERENCE TO MUTUAL INTERFERENCE

By Alex Goodman

Langley Aeronautical Laboratory
Langley Field, Va.

Washington
October 1951

AFMDC
TECHNICAL LIBRARY
AFL 2811

TECH LIBRARY KAFB, NM

0065506

NATIONAL ADVISORY COMMITTEE FOR AERONAUTICS

TECHNICAL NOTE 2504

EFFECTS OF WING POSITION AND HORIZONTAL-TAIL POSITION ON THE STATIC STABILITY CHARACTERISTICS OF MODELS WITH UNSWEPT AND 45° SWEPTBACK SURFACES WITH SOME REFERENCE TO MUTUAL INTERFERENCE

By Alex Goodman

SUMMARY

An investigation was made to determine the effects of wing position and horizontal-tail position on the low-speed static longitudinal and static lateral stability characteristics of airplane models having unswept and 45° sweptback surfaces.

The results indicated that both the unswept and the sweptback low-wing low-horizontal-tail configurations were the optimum configurations from the standpoint of longitudinal and lateral stability. The results indicated that, for all wing positions, moving the horizontal tail from the high to the low position resulted in configurations which were longitudinally stable throughout the angle-of-attack range. For the lateral case, the vertical-tail contribution to the directional stability was increased by moving the wing from the high to the low position because of the favorable sidewash at the vertical tail arising from the wing-fuselage interference. The addition of a horizontal tail in the low position produced a further increase in directional stability. The results also indicated that at low angles of attack the effective dihedral due to wing-fuselage interference increased as the wing height was increased - that is, from approximately -4° for the low-wing configuration to 5° for the high-wing configuration. This effect could be predicted with fair accuracy by available theory.

At low angles of attack, the lateral force on the fuselage was increased because of the end-plate effect when a wing was placed in the high or the low position. However, the lateral force on the fuselage decreased for the low-wing configuration and increased for the high-wing configuration as the angle of attack was increased because of the variation in the distribution of sidewash on the fuselage with angle of attack.

INTRODUCTION

Many changes in the design of major components of airplanes have been made necessary in order to fulfill the demands of high-speed flight. Several of the more important changes have been the incorporation of large amounts of sweep in the wing and tail surfaces and changes in wing and horizontal-tail positions relative to the fuselage. These changes have led to considerations of some configurations for which design information regarding stability characteristics is not available. Much information is available on the influence of the wing, fuselage, and tail geometry on the static stability characteristics of unswept high-aspect-ratio configurations (for example, references 1 to 4). In order to provide similar information for present-day-airplane designs, a series of investigations is being conducted in the Langley stability tunnel on models having various interchangeable parts. Results of investigations made to determine the effect of location of a swept horizontal tail and the effect of vertical-tail size and vertical-tail length on the static stability characteristics are presented in references 5 and 6, respectively.

The present investigation was made to determine the effects of wing position and horizontal-tail position (relative to fuselage center line) on the static stability characteristics of models with unswept and 45° sweptback surfaces. These models are representative of present-day high-speed airplanes. The data obtained from this investigation have been used to determine interference effects between the fuselage and horizontal tail and between the wing and fuselage and to determine the interference effects of the wing-fuselage combination on the contribution of the horizontal and vertical tails to the static-stability parameters. Also, an efficiency factor of the vertical tail as a function of wing position has been determined.

SYMBOLS

The data presented are in the form of standard NACA coefficients of forces and moments which are referred to the stability system of axes, with the origin at the projection on the plane of symmetry of the calculated aerodynamic center of the wing. The positive direction of the forces, moments, and angular displacements are shown in figure 1. The coefficients and symbols are defined as follows:

C_L lift coefficient $\left(L/qS_W\right)$

C_X longitudinal-force coefficient $\left(X/qS_W\right)$ $\left(\text{at } \psi = 0^{\circ},\ C_X = -C_D\right)$

C_Y	lateral-force coefficient $\left(Y/qS_W\right)$
C_D	drag coefficient $\left(D/qS_W\right)$
C_l	rolling-moment coefficient $\left(L'/qS_W b_W\right)$
C_m	pitching-moment coefficient $\left(M/qS_W \bar{c}_W\right)$
C_n	yawing-moment coefficient $\left(N/qS_W b_W\right)$
L	lift; in figure 1(a), $L = -Z$
Z	normal force
X	longitudinal force $\left(\text{at } \psi = 0^\circ,\ X = -D\right)$
D	drag
Y	lateral force
L'	rolling moment
M	pitching moment
N	yawing moment
q	dynamic pressure (free stream unless otherwise noted) $\left(\rho V^2/2\right)$
ρ	mass density of air
V	free-stream velocity
b	span, measured perpendicular to fuselage center line
S	area
c	chord, measured parallel to fuselage center line
A	aspect ratio (b^2/S)
A_e	effective aspect ratio, corresponding to theoretical lift-curve slope
$\bar{c}$	mean aerodynamic chord
$\bar{x}$	chordwise distance from leading edge of root chord to quarter chord of wing mean aerodynamic chord
l	tail length, distance parallel to fuselage center line from $\bar{c}/4$ of wing to $\bar{c}/4$ of tail

Z_W wing height, perpendicular distance from fuselage center line to wing chord plane (positive when wing is above fuselage center line)

Z_H horizontal-tail height, perpendicular distance from fuselage center line to horizontal-tail chord plane

d maximum diameter of fuselage

λ taper ratio $\left(\frac{\text{Tip chord}}{\text{Root chord}}\right)$

α angle of attack of wing (unless otherwise noted), degrees

ψ angle of yaw, degrees (for force tests, $\psi = -\beta$)

β angle of sideslip, degrees

Λ angle of sweepback of quarter-chord line, degrees

Γ effective dihedral angle, degrees

$\frac{\partial\epsilon}{\partial\alpha}$ rate of change of effective downwash angle at horizontal tail with angle of attack

σ effective sidewash angle at vertical tail (positive when tends to decrease angle of attack of vertical tail), degrees

$\frac{\partial\sigma}{\partial\psi}$ rate of change of effective sidewash angle at vertical tail with angle of yaw

$\left(1 - \frac{\partial\sigma}{\partial\psi}\right)\frac{q_V}{q}$ efficiency factor of vertical tail in presence of wing fuselage

$C_{L_{max}}$ maximum lift coefficient

$C_{m_\alpha} = \frac{\partial C_m}{\partial\alpha}$, per degree

$C_{L_{\alpha V}}$ lift-curve slope of vertical tail $\left(C_L\right.$ of vertical tail based on vertical-tail area$\left.\right)$, per degree $\left(\frac{\partial C_{L_V}}{\partial\alpha}\right)$

$C_{L_{\alpha_H}}$ lift-curve slope of horizontal tail (C_L of horizontal tail based on horizontal-tail area), per degree $\left(\frac{\partial C_{L_H}}{\partial \alpha}\right)$

C_{Y_ψ} lateral-force parameter, per degree $\left(\left(\frac{\partial C_Y}{\partial \psi}\right)_{\psi=0}\right)$

C_{n_ψ} directional-stability parameter, per degree $\left(\left(\frac{\partial C_n}{\partial \psi}\right)_{\psi=0}\right)$

C_{l_ψ} effective-dihedral parameter, per degree $\left(\left(\frac{\partial C_l}{\partial \psi}\right)_{\psi=0}\right)$

ΔC_{Y_ψ}, ΔC_{n_ψ}, ΔC_{l_ψ} contribution of vertical tail to derivatives C_{Y_ψ}, C_{n_ψ}, and C_{l_ψ} in presence of wing-fuselage combinations; that is, $\Delta C_{Y_\psi} = C_{Y_{\psi_{W+F+V}}} - C_{Y_{\psi_{W+F}}}$

$\Delta_1 C_{Y_\psi}$, $\Delta_1 C_{n_\psi}$, $\Delta_1 C_{l_\psi}$, $\Delta_1 C_m$ increments of coefficients caused by wing-fuselage interference; that is, $\Delta_1 C_{Y_\psi} = C_{Y_{\psi_{W+F}}} - \left(C_{Y_{\psi_W}} + C_{Y_{\psi_F}}\right)$

$\Delta_2 C_{Y_\psi}$, $\Delta_2 C_{n_\psi}$, $\Delta_2 C_{l_\psi}$ increments of coefficients caused by wing-fuselage interference on vertical-tail contribution or on complete-tail contribution; that is, for horizontal tail off $\Delta_2 C_{Y_\psi} = \left(C_{Y_{\psi_{W+F+V}}} - C_{Y_{\psi_{W+F}}}\right) - \left(C_{Y_{\psi_{F+V}}} - C_{Y_{\psi_F}}\right)$

and for horizontal tail on

$$\Delta_2 C_{Y_\psi} = \left(C_{Y_{\psi_{W+F+V+H}}} - C_{Y_{\psi_{W+F}}}\right) - \left(C_{Y_{\psi_{F+V+H}}} - C_{Y_{\psi_F}}\right)$$

$\Delta_3 C_{Y_\psi}$, $\Delta_3 C_{n_\psi}$, $\Delta_3 C_{l_\psi}$ increments of coefficients caused by fuselage interference on vertical-tail contribution or on complete-tail contribution; that is, for horizontal tail off

$$\Delta_3 C_{Y_\psi} = \left(C_{Y_{\psi_{F+V}}} - C_{Y_{\psi_F}}\right) - C_{Y_{\psi_V}}$$

and for horizontal tail on

$$\Delta_3 C_{Y_\psi} = \left(C_{Y_{\psi_{F+V+H}}} - C_{Y_{\psi_F}}\right) - C_{Y_{\psi_{V+H}}}$$

$\Delta_2 C_m$ increment of coefficient caused by wing-fuselage interference on horizontal-tail contribution; that is,

$$\Delta_2 C_m = \left(C_{m_{W+F+V+H}} - C_{m_{W+F+V}}\right) - \left(C_{m_{F+V+H}} - C_{m_{F+V}}\right)$$

$\Delta_3 C_m$ increment of coefficient caused by fuselage interference on horizontal-tail contribution; that is,

$$\Delta_3 C_m = \left(C_{m_{F+V+H}} - C_{m_{F+V}}\right) - C_{m_H}$$

Subscripts and abbreviations:

W	isolated wing
W_1, W_2, W_3	wing positions relative to fuselage (see fig. 2)
F	fuselage
V	vertical tail
H	isolated horizontal tail
H_1, H_2	horizontal-tail positions relative to fuselage (see fig. 2)
r	root
t	tip
X', Y', Z'	components along body axes
σ	component due to sidewash

APPARATUS AND MODELS

The tests of the present investigation were conducted in the 6- by 6-foot test section of the Langley stability tunnel.

Plan and elevation views of the complete models, having unswept and sweptback surfaces, showing the various wing and horizontal-tail positions

are presented in figure 2. A list of the pertinent geometric characteristics of the various component parts is given in table I.

The fuselage was a body of revolution having a circular-arc profile with a blunt tail end (fineness ratio of 6.90). The wings and horizontal tails had an aspect ratio of 4.0, a taper ratio of 0.6, and an NACA 65A008 profile in sections parallel to the plane of symmetry. The vertical tails were of the same taper ratio and airfoil section but had an aspect ratio of 2.0. The quarter-chord lines were swept back 0° and 45° for the unswept and swept surfaces, respectively. Ordinates for the NACA 65A008 section and for the fuselage are given in tables II and III, respectively. All parts were constructed of mahogany.

The complete models used for the present investigation were designed to permit tests of the wing alone, the fuselage alone, the wing-fuselage combination (with the wing at several different heights), or the fuselage in combination with any of the several tail configurations with or without the wings. A complete list of the configurations investigated is presented in table IV.

The models were mounted on a single strut at the point shown in figure 2. Forces and moments were measured by means of a six-component balance system. Photographs of two of the configurations tested are presented as figure 3. All lifting surfaces were set at 0° incidence with respect to the fuselage center line.

TESTS

Tests were made at a dynamic pressure of 39.8 pounds per square foot which corresponds to a Mach number of about 0.17 and a Reynolds number of 0.88×10^{6} based on the mean aerodynamic chord of the wings. The models were tested through an angle-of-attack range from about -2° up to and beyond the angle of maximum lift at angles of yaw of 0° and $\pm 5^{\circ}$. Tare tests were made at $\psi = 0^{\circ}$ in order to determine the effects of the support-strut interference on the C_L, C_X, and C_m data for the unswept wing alone and for all configurations with swept surfaces.

CORRECTIONS

Approximate corrections, based on unswept-wing theory, for the effects of jet boundaries (reference 7) have been applied to the angle of attack and longitudinal-force coefficient. The data have also been corrected for the effects of blocking by the method given in reference 8.

Corrections for the effects of support-strut interference have been applied to C_X and C_m. The tares determined for the swept configurations were also applied to the unswept configurations since the tares determined for the unswept and swept wings were similar. The effect of support-strut interference on C_L was found to be negligible for these tests and, therefore, the tare corrections were not applied.

METHODS OF ANALYSIS

The results of the present investigation are analyzed in terms of the individual contributions of the various parts of the models to the aerodynamic characteristics and to the more important interference effects.

Longitudinal-Stability Case

In accordance with conventional procedures (for example, as outlined in reference 1), the pitching-moment coefficient for the complete airplane can be expressed as

$$C_m = C_{m_W} + C_{m_F} + \Delta_1 C_m + \Delta_2 C_m + C_{m_H} + \Delta_3 C_m \tag{1}$$

The subscripts W, F, and H refer to the isolated wing, the fuselage, and the horizontal tail, respectively. The increments expressed by $\Delta_1 C_m$, $\Delta_2 C_m$, and $\Delta_3 C_m$ denote, respectively, the mutual interference of the wing-fuselage combination, the interference of the wing-fuselage combination on the horizontal-tail contribution, and the interference of the fuselage on the horizontal-tail contribution. These increments can be obtained from the test results in the manner illustrated by the following equations:

$$\Delta_1 C_m = C_{m_{W+F}} - \left(C_{m_W} + C_{m_F}\right) \tag{2}$$

$$\Delta_2 C_m = \left(C_{m_{W+F+V+H}} - C_{m_{W+F+V}}\right) - \left(C_{m_{F+V+H}} - C_{m_{F+V}}\right) \tag{3}$$

$$\Delta_3 C_m = \left(C_{m_{F+V+H}} - C_{m_{F+V}}\right) - C_{m_H} \tag{4}$$

Since the horizontal tail was not tested as an isolated surface, the parameter C_{m_H} was not determined directly. For this investigation,

however, the wing and horizontal tail were geometrically similar; therefore, C_{m_H} can be expressed in terms of the isolated wing characteristics as

$$C_{m_H} = \frac{S_H}{S_W}\left[C_{m_W} - C_{L_W}\left(\frac{l_H}{\bar{c}_W}\cos\alpha + \frac{Z_H}{\bar{c}_W}\sin\alpha\right) - C_{D_W}\left(\frac{l_H}{\bar{c}_W}\sin\alpha - \frac{Z_H}{\bar{c}_W}\cos\alpha\right)\right] \tag{5}$$

The value of C_{m_W} was included in equation (5) in order to account for the pitching moment obtained for the wings alone (see fig. 4).

The interference increments $\Delta_2 C_m$ and $\Delta_3 C_m$ can be used to evaluate the rate of change of downwash at the horizontal tail with angle of attack $\partial\epsilon/\partial\alpha$ for the low angle-of-attack range $(\alpha \approx 0^\circ)$. This parameter can be obtained from the test results by using equation (1) in the form

$$C_{m_\alpha} = C_{m_{\alpha_{W+F}}} + \Delta_2 C_{m_\alpha} + C_{m_{\alpha_H}} + \Delta_3 C_{m_\alpha}$$

where

$$\Delta_2 C_{m_\alpha} + C_{m_{\alpha_H}} + \Delta_3 C_{m_\alpha} = \left(1 - \frac{\partial\epsilon}{\partial\alpha}\right)\frac{S_H}{S_W}\frac{q_H}{q}\left(\frac{l_H}{\bar{c}_W}\cos\alpha + \frac{Z_H}{\bar{c}_W}\sin\alpha\right)C_{L_{\alpha_H}}$$

For the low angle-of-attack range, the ratio q_H/q can be assumed to be 1.0. Solving for $\partial\epsilon/\partial\alpha$ gives

$$\frac{\partial\epsilon}{\partial\alpha} = 1 - \frac{\Delta_2 C_{m_\alpha} + C_{m_{\alpha_H}} + \Delta_3 C_{m_\alpha}}{C_{L_{\alpha_H}}\frac{S_H}{S_W}\frac{l_H}{\bar{c}_W}}$$

but $C_{L_{\alpha_H}}\frac{S_H}{S_W}\frac{l_H}{\bar{c}_W} = C_{m_{\alpha_H}}$, and the values of $\Delta_2 C_{m_\alpha}$ and $\Delta_3 C_{m_\alpha}$ can be obtained from equations (3) and (4), respectively. Therefore,

$$\frac{\partial\epsilon}{\partial\alpha} = \frac{C_{m_{\alpha_H}} - \left(C_{m_{\alpha_{W+F+V+H}}} - C_{m_{\alpha_{W+F+V}}}\right)}{C_{m_{\alpha_H}}} \tag{6}$$

Lateral-Stability Case

By using a method analogous to the one employed for the longitudinal-stability case, the static-lateral-stability derivatives of a complete airplane can be expressed as (see reference 1)

$$C_{Y_\psi} = C_{Y_{\psi_W}} + C_{Y_{\psi_F}} + \Delta_1 C_{Y_\psi} + C_{Y_{\psi_{V+H}}} + \Delta_2 C_{Y_\psi} + \Delta_3 C_{Y_\psi} \tag{7}$$

$$C_{n_\psi} = C_{n_{\psi_W}} + C_{n_{\psi_F}} + \Delta_1 C_{n_\psi} + C_{n_{\psi_{V+H}}} + \Delta_2 C_{n_\psi} + \Delta_3 C_{n_\psi} \tag{8}$$

$$C_{l_\psi} = C_{l_{\psi_W}} + C_{l_{\psi_F}} + \Delta_1 C_{l_\psi} + C_{l_{\psi_{V+H}}} + \Delta_2 C_{l_\psi} + \Delta_3 C_{l_\psi} \tag{9}$$

The subscripts W, F, V, and V + H refer to the isolated wing, the fuselage, the vertical tail, and the vertical tail in the presence of the horizontal tail, respectively.

The interference increments can be obtained from the test results in a manner analogous to that used for the longitudinal-stability case. For example,

$$\Delta_1 C_{Y_\psi} = C_{Y_{\psi_{W+F}}} - \left(C_{Y_{\psi_W}} - C_{Y_{\psi_F}}\right) \tag{10}$$

$$\Delta_2 C_{Y_\psi} = \left(C_{Y_{\psi_{W+F+V+H}}} - C_{Y_{\psi_{W+F}}}\right) - \left(C_{Y_{\psi_{F+V+H}}} - C_{Y_{\psi_F}}\right) \tag{11}$$

For the lateral-stability case, the interference of the fuselage on the vertical-tail contributions $\Delta_3 C_{Y_\psi}$, $\Delta_3 C_{n_\psi}$, and $\Delta_3 C_{l_\psi}$ cannot be determined readily from measured results because it would necessitate acquiring measured values of the lateral-stability derivatives for the isolated vertical tail.

The contribution of the vertical tail to the lateral-stability parameters can be expressed in terms of an efficiency factor. The efficiency factor can be evaluated from the test results by using equation (7) in the form

$$C_{Y_\psi} = C_{Y_{\psi_{W+F}}} + C_{L_{\alpha_V}} \frac{S_V}{S_W}\left(1 - \frac{\partial\sigma}{\partial\psi}\right)\frac{q_V}{q}$$

where

$$C_{L_{\alpha_V}} \frac{S_V}{S_W} \left(1 - \frac{\partial\sigma}{\partial\psi}\right) \frac{q_V}{q} = \left(C_{Y_{\psi_{V+H}}} + \Delta_3 C_{Y_\psi}\right) + \Delta_2 C_{Y_\psi} \tag{12}$$

Solving for the efficiency factor $\left(1 - \frac{\partial\sigma}{\partial\psi}\right)\frac{q_V}{q}$ gives

$$\left(1 - \frac{\partial\sigma}{\partial\psi}\right)\frac{q_V}{q} = \frac{C_{Y_{\psi_{W+F+V+H}}} - C_{Y_{\psi_{W+F}}}}{C_{L_{\alpha_V}} \frac{S_V}{S_W}}$$

but $C_{L_{\alpha_V}} \frac{S_V}{S_W} = C_{Y_{\psi_{F+V+H}}} - C_{Y_{\psi_F}}$; therefore, for horizontal tail on

$$\left(1 - \frac{\partial\sigma}{\partial\psi}\right)\frac{q_V}{q} = \frac{C_{Y_{\psi_{W+F+V+H}}} - C_{Y_{\psi_{W+F}}}}{C_{Y_{\psi_{F+V+H}}} - C_{Y_{\psi_F}}} \tag{13}$$

and for horizontal tail off

$$\left(1 - \frac{\partial\sigma}{\partial\psi}\right)\frac{q_V}{q} = \frac{C_{Y_{\psi_{W+F+V}}} - C_{Y_{\psi_{W+F}}}}{C_{Y_{\psi_{F+V}}} - C_{Y_{\psi_F}}} \tag{14}$$

LIMITATIONS OF RESULTS

The interference increments obtained by the foregoing procedures are usually assumed to apply to airplanes having configurations which are similar to those of the models used in evaluating the increments.

Because of a slight asymmetry of the wings, a small amount of lift was obtained at zero angle of attack, although the wings had symmetrical airfoil sections (fig. 4). This asymmetry will affect the magnitude of the interference increments $\Delta_1 C_m$ and $\Delta_3 C_m$ (equations (2) and (4)) at zero angle of attack; however, the trends shown by these increments are believed to be reliable.

The present results should be applicable to full-scale results only for the angle-of-attack range before flow separation occurs. An increase

in Reynolds number would be expected to extend the linear range of the data to higher angles of attack.

RESULTS AND DISCUSSION

Presentation of Results

The static longitudinal stability characteristics of the various configurations investigated are given in figures 4 to 13 and the static lateral stability characteristics are presented in figures 14 to 29. A summary of the configurations investigated and of the figures that present the basic data for these configurations is given in table IV.

Static Longitudinal Stability Characteristics

Wing characteristics.- The lift, longitudinal-force, and pitching-moment data for the unswept and 45° sweptback wings of the present investigation are presented in figure 4. The values of the experimental lift-curve slopes, taken through zero angle of attack, of 0.0620 and 0.0545 are in fairly close agreement with the theoretical values of 0.0645 and 0.0530 given for the unswept wing and the 45° sweptback wing, respectively, in reference 9. At low angles of attack the aerodynamic centers of the wings are located at about 24.9 percent ($\Lambda = 0°$) and 25.2 percent ($\Lambda = 45°$) of the mean aerodynamic chord. The theoretical values given in reference 9 for the unswept and 45° sweptback wings are 25 percent and 26 percent, respectively. The variation of C_m with α obtained with the unswept and 45° sweptback wings is linear for the angle-of-attack range before flow separation occurs (approximately up to $\alpha = 8°$ as indicated in fig. 4). At the angle of attack at which flow separation occurs, an abrupt change in the C_{m_α} variations for both wings is obtained. In the case of the unswept wing, C_{m_α} becomes highly negative (stabilizing); whereas, for the 45° sweptback wing, C_{m_α} becomes positive (destabilizing).

Many of the aerodynamic parameters of a complete airplane are dependent to some extent on the character of flow over the wing; therefore, some consideration must be given to the angle-of-attack range over which the flow does not separate from the wing. As pointed out in reference 10, an indication of the limit of this range can be obtained by locating the initial break in the drag index curve $C_D - \frac{C_L^2}{\pi A_W}$ against angle of attack. A plot of this increment for the 45° sweptback wing can be obtained from

figure 15 of reference 6. The figure shows a break in the curve at about 7°. A similar break in the drag index curve occurs at about the same angle for the unswept wing. Corresponding breaks in the curves of the aerodynamic characteristics of combinations including the wings are to be expected at about this same angle of attack. For example, the breaks in the C_{l_ψ} variation with α obtained for the wing alone occurs at about $\alpha = 6^{\circ}$ and for the C_{m_α} variation obtained for the wings alone, at about $\alpha = 8^{\circ}$. An increase in Reynolds number would be expected to extend the angle-of-attack range before flow separation occurs.

Fuselage and fuselage-tail characteristics.- One of the main effects of the isolated fuselage on the static longitudinal stability is the contribution of an unstable pitching moment as shown in figure 5. As can be seen, the instability in pitch decreases as the angle of attack increases. The addition of a vertical tail to the fuselage did not change the static longitudinal stability characteristics. The main effect caused by the addition of either the unswept or 45° sweptback horizontal tail to the fuselage - vertical-tail combination is to produce a stable C_{m_α} variation at low and moderate angles of attack. An increment in pitching-moment coefficient exists between both the unswept and 45° sweptback low-horizontal-tail (H_1) and high-horizontal-tail (H_2) configurations (see fig. 5) for a greater part of the angle-of-attack range. Part of this increment probably is attributable to the fact that the air flow tends to follow the contour of the fuselage and hence has a downward-velocity component over the horizontal tail surface (H_2). At high angles of attack, the values of C_{m_α} decrease for both the unswept and swept fuselage - horizontal-tail combinations. In the case of the unswept configurations, C_{m_α} becomes neutrally stable for the low-horizontal-tail configuration and unstable for the high-horizontal-tail configuration. For the 45° sweptback configurations, at high angles of attack, C_{m_α} remains stable but to a lesser degree than at low angles of attack. The values of the interference increment $\Delta_3 C_m$ obtained for the two horizontal-tail positions as affected by the fuselage are presented in figure 10 and were obtained by the procedure explained in the section entitled "Methods of Analysis." The value of $\Delta_3 C_m$ at zero angle of attack obtained for the high horizontal tail probably results, as stated previously, from the fact that the streamlines of the flow tend to follow the fuselage contour. The reason that the value of $\Delta_3 C_m$ for the swept low-horizontal-tail configuration is not zero at $\alpha = 0^{\circ}$ has been discussed in the section entitled "Limitations of Results." At high angles of attack, the values of $\Delta_3 C_m$ decrease for both unswept and

swept configurations and in some cases become negative (favorable interference). Also at high angles of attack the unstable moment of the fuselage has increased. These effects, in addition to the decrease in C_{m_H} at high angles of attack (equation (5)), result in a decrease in the values of C_{m_α} for both the unswept and swept fuselage-tail combinations at high angles of attack. The decrease in $C_{m_{\dot{\alpha}}}$ at high angles of attack is greater for the high-horizontal-tail than for the low-horizontal-tail configurations since the interference increment $\Delta_3 C_m$ is less stabilizing (compare figs. 5 and 10).

Wing-fuselage characteristics.- The addition of a 45° swept wing in the mid, high, or low positions (W_1, W_2, or W_3, respectively) to the fuselage produced C_{m_α} characteristics similar to that obtained for the wing alone (see figs. 4 and 6). For the unswept wing configurations, the contribution of the fuselage at low angles of attack to the pitching-moment characteristics has a destabilizing effect. A small amount of wing-fuselage interference $\left(\Delta_1 C_m\right)$ which can probably be attributed to the rearward location of the wing-fuselage juncture is thereby indicated. A similar result (an increase of the unstable pitching-moment contribution of the wing-fuselage combination with a rearward shift of the wing-fuselage juncture) was obtained in reference 4 for an unswept midwing configuration. For the sweptback wing configurations at low angles of attack, the wing-fuselage interference cancels the usual unstable pitching-moment contribution of the fuselage. Apparently this effect is due to the fact that there is a loss in lift over the wing center section because of the fuselage interference. In the case of the sweptback wing, this loss occurs over sections of the wing which are forward of the aerodynamic center and results in a stabilizing moment. At high angles of attack, the contribution of the C_{m_W} to the pitching-moment characteristics of the wing-fuselage combinations predominates (favorable interference) and results in pitching moment trends which are similar to those of the wing alone (compare figs. 4 and 6).

The wing-fuselage interference increment $\Delta_1 C_m$ evaluated from the basic data by the procedures explained in the section entitled "Methods of Analysis" is presented in figure 11. The fact that $\Delta_1 C_m$ for the midwing configurations is not zero at $\alpha = 0^\circ$ is probably due to a slight asymmetry of the wings. (See the section entitled "Limitations of Results.") The trends of $\Delta_1 C_m$ shown in figure 11 are in agreement with the results presented in figure 6.

The lift-curve slope of the wing-fuselage configurations at $\alpha = 0^\circ$ was found to be slightly higher than that of the wing alone (see figs. 4

and 6). A similar result was obtained in reference 4 for a midwing configuration.

A comparison of $C_{L_{max}}$ obtained for the wings alone with $C_{L_{max}}$ for the wing-fuselage combinations indicates that the wing-fuselage interference increases $C_{L_{max}}$ for the unswept configurations but has a negligible effect for the swept configurations (compare figs. 4 and 6).

Complete-model characteristics.- The addition of a vertical tail to the wing-fuselage configurations had little effect on the longitudinal stability characteristics (see fig. 7). The low-horizontal-tail configurations produce stable C_{m_α} characteristics at the low angles of attack for all the wing heights with the exception of the unswept midwing configuration ($W_1 + F + V + H_1$) which exhibits a slightly unstable C_{m_α} variation (see fig. 8). Part of this result may be attributable to the fact that the downwash of the midwing configuration affects the low horizontal tail at low angles of attack since the low horizontal tail is very close to the center of the wing wake. For the high-wing and low-wing configurations, at low angles of attack, the center of the wing wake probably comes above and below the plane of the low horizontal tail. An illustration indicating the variation in location of the center of the wing wake with angle of attack for midwing, high-wing, and low-wing configurations is given in reference 11. At moderate angles of attack, a stable increase in C_{m_α} is obtained for all the unswept configurations, the midwing and high-wing configurations being more stable than the low-wing configuration. This result is probably due to the fact that a strong interference $\Delta_2 C_m$ exists between the low-wing - fuselage and the low-horizontal-tail configurations (strong downwash) since the low horizontal tail is close to the center of the wing wake at these angles of attack. For the sweptback configurations, a slight decrease in C_{m_α} (less stable) is obtained at moderate angles of attack. The decrease in C_{m_α} is smaller for the high-wing configuration (see fig. 8). This effect is probably due to the interference caused by the relative location of the center of the wing wake to the plane of the horizontal tail.

The effect of adding a high horizontal tail (H_2) to the unswept and swept wing-fuselage-tail configurations (see fig. 9) results in values of C_{m_α} which are more stable at low angles of attack than those obtained with the low horizontal tail (H_1). At moderate angles of attack, however, the high tail becomes ineffective and unstable variations of C_{m_α} result. The decrease in C_{m_α}, however, is smaller for the high-wing configurations.

The pitching-moment data of figures 5 to 9 have been used to determine the wing-fuselage interference on the horizontal tail $\Delta_2 C_m$ by the procedure explained in the section entitled "Methods of Analysis." The interference increment $\Delta_2 C_m$ for each wing height and horizontal tail height is presented in figure 12 for both the unswept and sweptback configurations and these results summarize the effects of the wing position and horizontal-tail position on the static longitudinal stability indicated by the preceding discussion. For the configurations investigated the low horizontal tails contribute more to the longitudinal stability at high angles of attack than the high horizontal tails because of the smaller wing-fuselage interference (compare figs. 8, 9, and 10). The values of the slopes $\partial\epsilon/\partial\alpha$ obtained by the procedure explained in the section entitled "Methods of Analysis," presented in figure 13, indicate the opposite effect at low angles of attack. In general, at low angles of attack, the closer the horizontal tail is to the center of the wing wake the greater the wing-fuselage interference on the horizontal tail (downwash increased). Also, at low angles of attack the wing-fuselage interference on the horizontal tail decreases as the sweep angle is increased (downwash decreased). A similar result for low angles of attack was obtained in reference 12 for unswept and 45° sweptback midwing configurations (see fig. 13).

Static Lateral Stability Characteristics

Wing characteristics.- The variations of C_{Y_ψ}, C_{n_ψ}, and C_{l_ψ} with angle of attack for the unswept and 45° sweptback wings are presented in figure 14. The flow separation indicated by the breaks in the drag index curves of reference 6 is further indicated by the breaks in C_{l_ψ} at about the same angles of attack. In the case of the unswept wing, C_{l_ψ} continues to increase as the angle of attack increases. This effect is probably attributable to the fact that, for the present unswept wing, local stalling of the center section occurs at low angles of attack (as indicated by break in drag index). This stall progresses outboard as the angle of attack is increased, one semispan of the wing being affected more than the other, and results in an increase in rolling moment. The derivatives C_{Y_ψ} and C_{n_ψ} are generally small for most of the angle-of-attack range. The values of C_{n_ψ} for the swept wing become positive (directionally unstable) at the high angles of attack.

The values of the slopes $\partial C_{l_\psi}/\partial C_L$ through $\alpha = 0°$ for the unswept and 45° sweptback wings are in reasonably good agreement with the values

calculated by the methods of reference 13. A comparison of the measured and calculated values of $\partial C_{l_\psi}/\partial C_L$ is presented in the following table:

Λ (deg)	$\partial C_{l_\psi}/\partial C_L$	
	Measured	Calculated
0	0.0011	0.0009
45	.0049	.0040

Fuselage and fuselage-tail characteristics.- The main contribution of the fuselage to the static lateral stability characteristics is an unstable yawing moment throughout the angle-of-attack range (see fig. 15). The addition of a vertical tail to the fuselage contributes a stable yawing moment for both unswept and swept configurations.

The addition of a horizontal tail in the low position (H_1) to the fuselage - vertical-tail combination generally increases C_{Y_ψ} and C_{n_ψ} slightly at $\alpha_H = 0^\circ$ for both the unswept and swept configurations. This increase in the parameters is due mainly to the increase in effective aspect ratio of the vertical tail caused by the end-plate effect of the horizontal tail. With the horizontal tail in the high position (H_2), a slightly adverse effect results; that is, the combination of the vertical and horizontal tails produced smaller increments in the parameters than the vertical tails alone (see fig. 15). The effective aspect ratios of the unswept and swept tails as determined by the procedure of reference 6 are presented in figure 21 in the form of the ratio $\frac{(A_{eV})_{H\ on}}{(A_{eV})_{H\ off}}$ plotted against the horizontal-tail-height ratio Z_H/b_V for $\alpha_H = 0^\circ$ and are compared with the results of reference 3. The results of figure 21 illustrate the effects on the derivatives C_{Y_ψ} and C_{n_ψ} just discussed. A similar result was obtained in reference 5.

The positive increase in C_{l_ψ} at $\alpha_H = 0^\circ$ (fig. 15) is provided by the vertical tail. As the angle of attack is increased, the vertical distance between the horizontal tail center of pressure and the roll axis decreases; thereby a decrease of C_{l_ψ} with angle of attack results. The addition of the horizontal tail in the low position (H_1) resulted in a

smaller increase in C_{l_ψ} at $\alpha_H = 0^\circ$. With the tail in the high position (H_2), the value of C_{l_ψ} at $\alpha_H = 0^\circ$ was about the same as that obtained with the fuselage - vertical-tail configuration. These effects are probably due to the antisymmetrical load induced on the horizontal tail by the vertical tail. This antisymmetrical loading can be accounted for qualitatively (as was done in references 5 and 12) by considering the effects of the tip vortices of the vertical tail acting on the horizontal tail when the horizontal tail is at $\alpha_H = 0^\circ$ and the entire tail assembly is at an angle of yaw. With the horizontal tail in the low position (H_1), the tip vortex at the base of the vertical tail would be expected to have a predominant effect and would tend to produce a negative increment in C_{l_ψ}. For the high tail (H_2) the loads induced by the vertical tail on the horizontal tail tend to cancel.

Wing-fuselage characteristics.- In order to analyze the effect of wing position on the lateral stability characteristics, a qualitative analysis similar to the analysis presented in reference 12 will be made of the flow about a yawed high-wing - fuselage configuration. By resolving the free-stream velocity V into the component velocities $V_{X'}$, $V_{Y'}$, and $V_{Z'}$ (component velocities along body axis (see fig. 1(a)), it can be seen that the flow about the fuselage induced by the components $V_{X'}$ and $V_{Z'}$ produce symmetrical variations of angle of attack at the wing. The component velocity $V_{Y'}$, however, gives rise to an antisymmetrical variation in angle of attack; that is, the flow about the fuselage induces an upwash velocity on the advancing wing panel and a downwash on the opposite wing panel. This variation corresponds to a positive increment of lift on the advancing wing panel and a negative increment of lift on the opposite wing panel. Thus, for positive angles of yaw a positive rolling moment results (see fig. 1(b)). Employing the same analysis shows that for a low-wing configuration a negative rolling moment will be induced. For a midwing configuration this effect does not exist. In addition to this effect, for a yawed fuselage at low angles of attack, a high-wing or a low-wing configuration should increase the lateral force because of the end-plate effect of the wing (see reference 12). The C_{l_ψ} and C_{Y_ψ} results at low angles of attack of figure 16 are in agreement with the preceding analysis.

The incremental values of C_{l_ψ} (at $\alpha = 0^\circ$) for the unswept and swept configurations are presented in figure 22 as a function of wing-height ratio Z_W/d. The values of the slopes $\frac{\partial C_{l_\psi}}{\partial(Z_W/d)}$ for the present

configurations are in good agreement with the experimental results of the unswept and 45° sweptback untapered configurations ($A_W = 5.18$) presented in reference 14. These experimental results are compared in figure 22 with the results obtained from the theory of reference 15 and the empirical relation given in reference 16. The incremental values of C_{l_ψ} $(\alpha = 0^\circ)$ are also presented in terms of an effective dihedral angle in figure 22. The values of C_{l_ψ}/Γ (C_{l_ψ} per degree of effective dihedral) obtained from reference 17 are presented in the following table and are used to express C_{l_ψ} in terms of an effective dihedral angle Γ:

Λ (deg)	C_{l_ψ}/Γ	
	Figure 16	Reference 17
0	0.00016	0.00020
45	.00015	.00018

The effective dihedral angle increased from approximately -4° to 5° in going from a low-wing configuration to a high-wing configuration $\left(-Z_W/d \text{ to } Z_W/d\right)$. (See fig. 22.) A similar effect is indicated by the results of reference 1.

The wing-fuselage configurations are directionally unstable (fig. 16). The unstable yawing moment of the fuselage predominates for the low- and moderate-angle-of-attack range. For the unswept configurations at high angles of attack the wing-fuselage configurations become stable and the values of C_{n_ψ} are approximately the same as those obtained for the wing alone. For the swept configurations at high angles of attack, the unstable yawing moment of the fuselage predominates.

The wing-fuselage interference increments $\Delta_1 C_{Y_\psi}$, $\Delta_1 C_{n_\psi}$, and $\Delta_1 C_{l_\psi}$ determined by the procedures explained in the section entitled "Methods of Analysis" are presented in figure 23. In accordance with the preceding qualitative analysis, it can be seen that the wing-fuselage interference induces a positive increment of rolling moment for the high-wing configurations and a negative increment for the low-wing configurations at low angles of attack. For the midwing configurations, the wing-fuselage interference increment $\Delta_1 C_{l_\psi}$ is small and probably due to a slight asymmetry of the model. The interference increment $\Delta_1 C_{Y_\psi}$ is positive

at low angles of attack for both the high-wing and low-wing configurations. At high angles of attack the interference increment of the high-wing configuration attains large positive values, whereas $\Delta_1 C_{Y_\psi}$ for the low-wing configuration decreases and becomes negative. This variation with α can probably be attributed to the effects of the induced sidewash V_σ on the fuselage. A strong sidewash (stabilizing) exists above the center of the wing wake for the low-wing configuration and below the center of the wing wake for the high-wing configuration. Therefore, at small angles of attack the greater part of the fuselage of the low-wing configuration as well as the high-wing configuration is situated in a strong sidewash (stabilizing). As the angle of attack increases, the part of the fuselage area situated in the stabilizing sidewash decreases for the low-wing configuration and increases for the high-wing configuration because of the movement of the wing wake with angle of attack. (See reference 12.)

For the unswept wing configurations (W_1, W_2, and W_3), the interference increment $\Delta_1 C_{n_\psi}$ is small. The interference increment $\Delta_1 C_{n_\psi}$ for the swept configurations is, in general, small and erratic.

Complete-model characteristics.- The qualitative analysis of the effects of wing-fuselage interference given in the section entitled "Wing-fuselage characteristics" will be extended to include the effects of wing-fuselage interference on the vertical-tail contribution. As indicated in the preceding analysis, the lateral flow about the fuselage induces an antisymmetrical lift distribution over the wing. Actually this variation in lift caused by the fuselage is restricted to a small region at the center of the wing. In this region a large spanwise pressure gradient is produced on the wing (reference 12). In the case of the high-wing configuration under consideration this pressure gradient will induce a sidewash velocity as shown in figure 1(b). This sidewash velocity changes sign for the low-wing configuration and, in the case of the midwing configuration, it is zero. The sidewash velocity produced by yaw is proportional to the angle of yaw and is independent of the angle of attack. However, because the position of the vertical tail relative to the center of the wing wake changes with angle of attack, the effect of the sidewash velocity on the vertical-tail contribution will also vary with angle of attack since in passing through the wing wake the sidewash velocity changes direction. According to this analysis, it can be seen that in the case of a low-wing configuration, with the vertical tail above the center of the wing wake, the sidewash velocity will increase the vertical-tail contribution (increase directional stability) and for the high-wing configuration, will reduce the vertical-tail contribution (decrease directional stability) relative to the vertical-tail contribution of the midwing configuration.

In general, the vertical tail, at zero angle of attack of the wing, contributes increments of C_{Y_ψ}, C_{n_ψ}, and C_{l_ψ} to the wing-fuselage results equal to those obtained by the addition of the vertical tail to the fuselage alone. (Compare figs. 15 and 18.) Also, the effects of wing position on the vertical-tail contribution to the derivatives C_{Y_ψ}, C_{n_ψ}, and C_{l_ψ}, at low angles of attack, presented in figures 17 and 18 are in agreement with the preceding qualitative analysis. However, the explanation given in the preceding qualitative analysis does not account for the variations of the derivatives obtained at the moderate and high angles of attack. For the high-wing configurations the vertical-tail contribution ΔC_{n_ψ} decreases as the angle of attack increases and becomes zero for the unswept configuration and positive (destabilizing) for the swept configuration (see fig. 18). The unswept high-wing configuration is stable, however, because the wing-fuselage contribution to C_{n_ψ} is stable at high angles of attack (see figs. 16 and 17). For the swept high-wing configuration the unstable contributions of both the vertical tail and wing fuselage are additive and this results in a directionally unstable configuration. The vertical-tail contribution ΔC_{n_ψ} also decreases but remains stable at the high angles of attack for the midwing and low-wing configurations. The wing-fuselage contribution to C_{n_ψ}, however, predominates for the midwing configurations and results in a stable configuration for unswept surfaces and an unstable configuration for the swept surfaces. In the case of the low-wing configurations, the stable contribution of the vertical tail increases the stability of the unswept configuration and overcomes the unstable contribution of the swept wing-fuselage combination (see figs. 16 to 18).

The decreases in ΔC_{Y_ψ} and ΔC_{n_ψ} at the high angles of attack (not accounted for in the preceding analysis) indicate that an additional sidewash exists in the vicinity of the vertical tail which tends to cancel or reverse the sidewash due to the wing-fuselage interference. This additional sidewash at the vertical tail may be attributable to the lateral movement of the wing-tip vortices.

The results obtained by adding a horizontal tail in either the low (H_1) or high (H_2) positions to the wing-fuselage - vertical-tail configurations are presented in figures 19 and 20, respectively. In general, the low horizontal tail increases the contribution of the vertical tail because of the end-plate effect (see fig. 21). The results obtained with the high-horizontal-tail configuration are similar to those obtained with the horizontal tail off (see figs. 17, 19, and 20). The unstable contribution of the vertical tail to C_{n_ψ} for the swept high-wing

configuration at high angles of attack is reduced with the addition of the low horizontal tail even though the derivative C_{Y_ψ} is increased negatively (see fig. 19). This increase can probably be attributed to the downward and forward movement of the center of pressure of the vertical tail due to the end-plate effect of the horizontal tail, and a reduction of the moment arm results (reference 5).

The increments of wing-fuselage interference on the vertical-tail contributions $\Delta_2 C_{Y_\psi}$, $\Delta_2 C_{n_\psi}$, and $\Delta_2 C_{l_\psi}$ were evaluated from the basic data by the procedure explained in the section entitled "Methods of Analysis." These increments are presented in figures 24 to 26 for the horizontal-tail-off, low-horizontal-tail, and high-horizontal-tail configurations, respectively. In order to summarize these results the increment $\Delta_2 C_{Y_\psi}$ was used to evaluate an efficiency factor $\left(1 - \frac{\partial\sigma}{\partial\psi}\right)\frac{q_V}{q}$. (See section entitled "Methods of Analysis.") The variation of the efficiency factor with angle of attack is presented in figure 27. The average values of figure 27 are presented in figure 28 as a function of wing position and angle of attack for both the unswept and swept configurations. The values of the efficiency factor at low angles of attack are mainly due to the wing-fuselage interference. At high angles of attack the efficiency factor of the vertical tail decreases. Part of this reduction in the vertical-tail efficiency factor may be attributable, as mentioned previously, to the effects of the wing-tip vortices. At low angles of attack the effects of sweep on the efficiency factor are negligible. A similar conclusion can be drawn from the results of reference 12. A comparison of the efficiency factors for the unswept and swept midwing and low-wing configurations at $C_{L_{max}}$ (α approx. 15° and 21°, respectively), however, indicates an increase in the vertical-tail efficiency factor as the sweep angle increases. For the high-wing configurations, however, an increase in sweep results in a decrease in the vertical-tail efficiency factor at $C_{L_{max}}$.

Values of $\left(1 - \frac{\partial\sigma}{\partial\psi}\right)\frac{q_V}{q}$ at $\alpha = 0^\circ$ taken from figure 28 for the unswept and swept configurations are plotted against wing-height ratio in figure 29. The $\left(1 - \frac{\partial\sigma}{\partial\psi}\right)\frac{q_V}{q}$ results of the unswept configurations are compared with values of $\left(1 - \frac{\partial\sigma}{\partial\psi}\right)\frac{q_V}{q}$ obtained from the data of reference 18 for a circular-fuselage configuration and for a circular fuselage with a wedge-shaped-rear configuration. In general, the variations of $\left(1 - \frac{\partial\sigma}{\partial\psi}\right)\frac{q_V}{q}$ with wing height are similar to the results

of the present investigation. The wedge-shaped-rear fuselage configuration gives the best agreement probably because of the similarity of the fuselage shapes in the vicinity of the vertical tail.

CONCLUSIONS

Results of an investigation made to determine the effects of wing position and horizontal-tail position on the low-speed static longitudinal and static lateral stability characteristics of airplane models having unswept and 45° sweptback surfaces indicated the following conclusions:

1. For all wing positions, moving the horizontal tail from the high to the low position resulted in configurations which were longitudinally stable throughout the angle-of-attack range.

2. The vertical-tail contribution to the directional stability was increased by moving the wing from the high to the low position because of the favorable sidewash at the vertical tail arising from the wing-fuselage interference. The addition of a horizontal tail in the low position produced a further increase in directional stability.

3. As indicated by both available theory and results of previous investigations, the effective dihedral at low angles of attack caused by wing-fuselage interference increased as the wing height was increased - that is, from approximately -4° for the low-wing configuration to 5° for the high-wing configuration.

4. At low angles of attack, the lateral force on the fuselage was increased because of the end-plate effect when a wing was placed in the high or low position. However; the lateral force on the fuselage decreased for the low-wing configuration and increased for the high-wing configuration as the angle of attack was increased because of the variation in the distribution of sidewash on the fuselage with angle of attack.

Langley Aeronautical Laboratory
National Advisory Committee for Aeronautics
Langley Field, Va., July 11, 1951

REFERENCES

1. House, Rufus O., and Wallace, Arthur R.: Wind-Tunnel Investigation of Effect of Interference on Lateral-Stability Characteristics of Four NACA 23012 Wings, an Elliptical and a Circular Fuselage, and Vertical Fins. NACA Rep. 705, 1941.

2. Recant, Isidore G., and Wallace, Arthur R.: Wind-Tunnel Investigation of the Effect of Vertical Position of the Wing on the Side Flow in the Region of the Vertical Tail. NACA TN 804, 1941.

3. Murray, Harry E.: Wind-Tunnel Investigation of End-Plate Effects of Horizontal Tails on a Vertical Tail Compared with Available Theory. NACA TN 1050, 1946.

4. Jacobs, Eastman N., and Ward, Kenneth E.: Interference of Wing and Fuselage from Tests of 209 Combinations in the N.A.C.A. Variable-Density Tunnel. NACA Rep. 540, 1935.

5. Brewer, Jack D., and Lichtenstein, Jacob H.: Effect of Horizontal Tail on Low-Speed Static Lateral Stability Characteristics of a Model Having 45° Sweptback Wing and Tail Surfaces. NACA TN 2010, 1950.

6. Queijo, M. J., and Wolhart, Walter D.: Experimental Investigation of the Effect of Vertical-Tail Size and Length and of Fuselage Shape and Length on the Static Lateral Stability Characteristics of a Model with 45° Sweptback Wing and Tail Surfaces. NACA TN 2168, 1950.

7. Silverstein, Abe, and White, James A.: Wind-Tunnel Interference with Particular Reference to Off-Center Positions of the Wing and to the Downwash at the Tail. NACA Rep. 547, 1936.

8. Herriot, John G.: Blockage Corrections for Three-Dimensional-Flow Closed-Throat Wind Tunnels, with Consideration of the Effect of Compressibility. NACA Rep. 995, 1950. (Formerly NACA RM A7B28.)

9. DeYoung, John: Theoretical Additional Span Loading Characteristics of Wings with Arbitrary Sweep, Aspect Ratio, and Taper Ratio. NACA TN 1491, 1947.

10. Goodman, Alex, and Fisher, Lewis R.: Investigation at Low Speeds of the Effect of Aspect Ratio and Sweep on Rolling Stability Derivatives of Untapered Wings. NACA Rep. 968, 1950. (Formerly NACA TN 1835.)

11. Jacobs, W.: Calculation of the Induced Cross-Wind of Aircraft. British Ministry of Supply TPA3/TIB Translation No. GDC 10/400.T, Feb. 1943.

12. Schlichting, H.: Aerodynamics of the Mutual Influence of Aircraft Parts (Interference). Library Translation No. 275, British R.A.E., Oct. 1948.

13. Toll, Thomas A., and Queijo, M. J.: Approximate Relations and Charts for Low-Speed Stability Derivatives of Swept Wings. NACA TN 1581, 1948.

14. Möller, E.: Systematische Sechskomponentenmessungen an Flügel/Rumpfanordnungen mit Pfeilflügeln konstanter Tiefe. Forschungsbericht Nr. 1318/4, Deutsche Luftfahrtforschung (Braunschweig), 1943.

15. Multhopp, H.: Aerodynamics of the Fuselage. NACA TM 1036, 1942.

16. Campbell, John P., and McKinney, Marion O., Jr.: Summary of Methods for Calculating Dynamic Lateral Stability and Response and for Estimating Lateral Stability Derivatives. NACA TN 2409, 1951.

17. Bird, John D.: Some Theoretical Low-Speed Span Loading Characteristics of Swept Wings in Roll and Sideslip. NACA Rep. 969, 1950. (Formerly NACA TN 1839.)

18. Recant, I. G., and Wallace, Arthur R.: Wind-Tunnel Investigation of Effect of Yaw on Lateral-Stability Characteristics. IV - Symmetrically Tapered Wing with a Circular Fuselage Having a Wedge-Shaped Rear and a Vertical Tail. NACA ARR, March 1942.

TABLE I.- PERTINENT GEOMETRIC CHARACTERISTICS OF MODELS

Fuselage:		
Length, in.		41.38
Fineness ratio		6.90
Wings:		
Aspect ratio, A_W	4.0	4.0
Taper ratio, λ_W	0.6	0.6
Quarter-chord sweep angle, deg	0	45
Dihedral angle, deg	0	0
Twist, deg	0	0
NACA airfoil section	65A008	65A008
Area, S_W, sq in.	324	324
Span, b_W, in.	36	36
Mean aerodynamic chord, $\bar{c}_W$, in.	9.19	9.19
Wing-height ratio, Z_W/d	0, ±0.333	0, ±0.333
Vertical tails:		
Aspect ratio, A_V	2.0	2.0
Taper ratio, λ_V	0.6	0.6
Quarter-chord sweep angle, deg	0	45
NACA airfoil section	65A008	65A008
Area, S_V, sq in.	48.6	48.6
Span, b_V, in.	9.86	9.86
Mean aerodynamic chord, $\bar{c}_V$, in.	5.03	5.03
Tail length, l_V, in.	16.7	16.7
Area ratio, S_V/S_W	0.15	0.15
Tail-length ratio, l_V/b_W	0.464	0.464
Horizontal tails:		
Aspect ratio, A_H	4.0	4.0
Taper ratio, λ_H	0.6	0.6
Quarter-chord sweep angle, deg	0	45
Dihedral angle, deg	0	0
Twist, deg	0	0
NACA airfoil section	65A008	65A008
Area, S_H, sq in.	64.8	64.8
Span, b_H, in.	16.10	16.10
Mean aerodynamic chord, $\bar{c}_H$, in.	4.11	4.11
Area ratio, S_H/S_W	0.20	0.20
Area ratio, S_H/S_V	1.33	1.33
Tail length, l_H, in.	16.7	19.25
Tail-length ratio, $l_H/\bar{c}_W$	1.81	2.09
Tail height, Z_{H_1}, in.	0	0
Tail height, Z_{H_2}, in.	5.21	5.21
Tail-height ratio, Z_H/b_V	0, 0.528	0, 0.528

NACA

TABLE II.- ORDINATES FOR NACA 65A008 AIRFOIL

[Station and ordinates in percent airfoil chord]

Station	Ordinate
0	0
.50	.62
.75	.75
1.25	.95
2.50	1.30
5.00	1.75
7.50	2.12
10.00	2.43
15.00	2.93
20.00	3.30
25.00	3.59
30.00	3.79
35.00	3.93
40.00	4.00
45.00	3.99
50.00	3.90
55.00	3.71
60.00	3.46
65.00	3.14
70.00	2.76
75.00	2.35
80.00	1.90
85.00	1.43
90.00	.96
95.00	.49
100.00	.02
L.E. radius 0.408	

TABLE III.- FUSELAGE ORDINATES

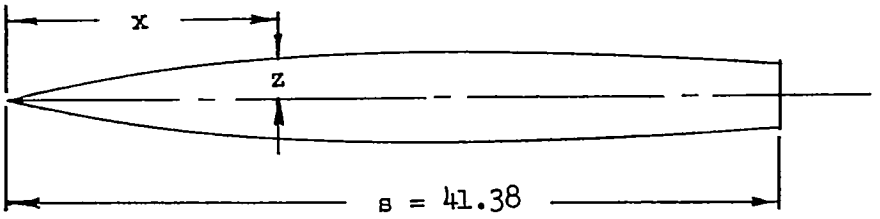

x/s	z/s
0	0
.025	.0070
.050	.0140
.075	.0200
.100	.0260
.125	.0320
.150	.0380
.200	.0480
.250	.0560
.300	.0620
.350	.0660
.400	.0700
.450	.0715
.500	.0724
.550	.0720
.600	.0710
.650	.0680
.700	.0650
.750	.0610
.800	.0560
.850	.0510
.900	.0450
.950	.0390
1.000	.0320

NACA

TABLE IV.- CONFIGURATIONS INVESTIGATED

45° sweptback-surface and unswept-surface configurations (a)	Basic data	Figure
F F + V F + V + H_1 F + V + H_2	C_L, C_m, C_X C_{Y_ψ}, C_{n_ψ}, C_{l_ψ}	5 15
W	C_L, C_m, C_X C_{Y_ψ}, C_{n_ψ}, C_{l_ψ}	4 14
W_1 + F W_2 + F W_3 + F	C_L, C_m, C_X C_{Y_ψ}, C_{n_ψ}, C_{l_ψ}	6 16
W_1 + F + V W_2 + F + V W_3 + F + V	C_L, C_m, C_X C_{Y_ψ}, C_{n_ψ}, C_{l_ψ}	7 17
W_1 + F + V + H_1 W_2 + F + V + H_1 W_3 + F + V + H_1	C_L, C_m, C_X C_{Y_ψ}, C_{n_ψ}, C_{l_ψ}	8 19
W_1 + F + V + H_2 W_2 + F + V + H_2 W_3 + F + V + H_2	C_L, C_m, C_X C_{Y_ψ}, C_{n_ψ}, C_{l_ψ}	9 20

[a]Notation (for details, see fig. 2):

W_1, W_2, W_3 wing positions

F fuselage

V vertical tail

H_1, H_2 horizontal-tail positions

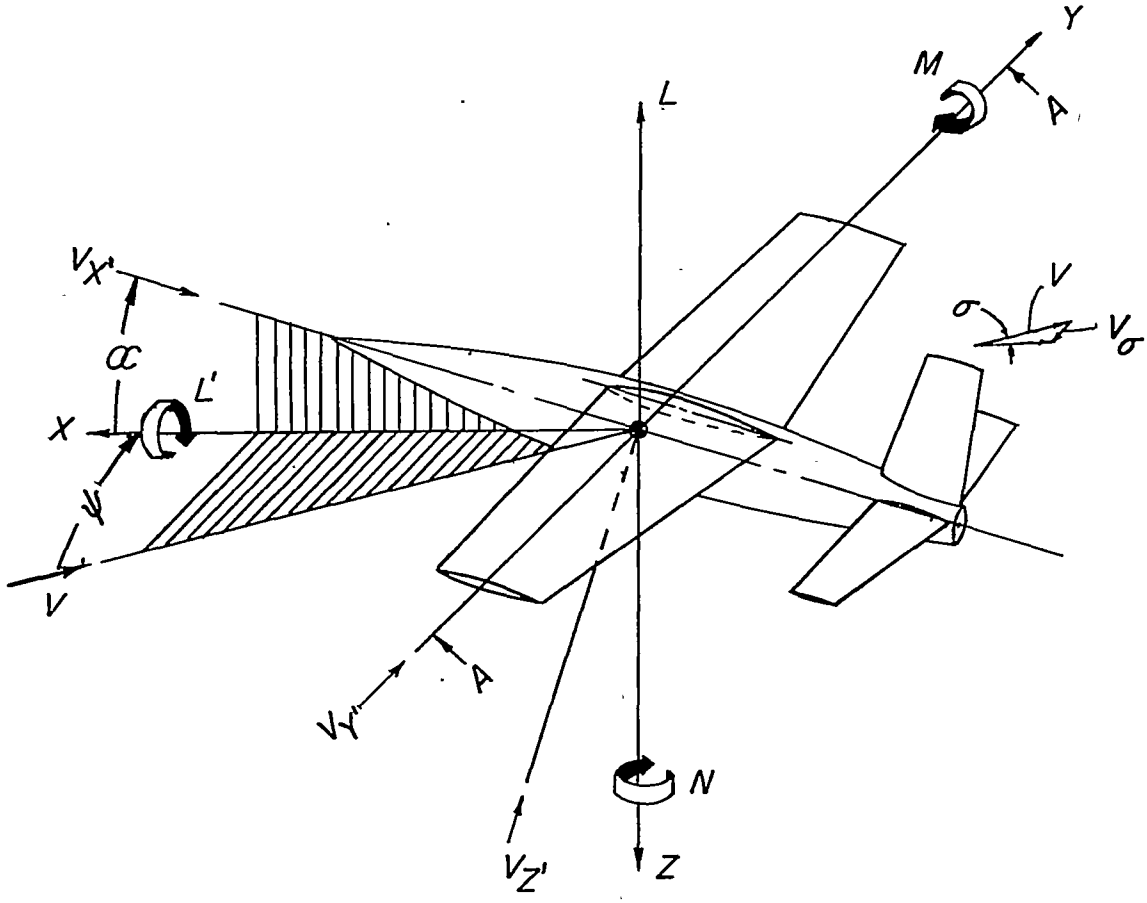

(a) System of axes used. Arrows indicate positive direction of angles, velocities, forces, and moments.

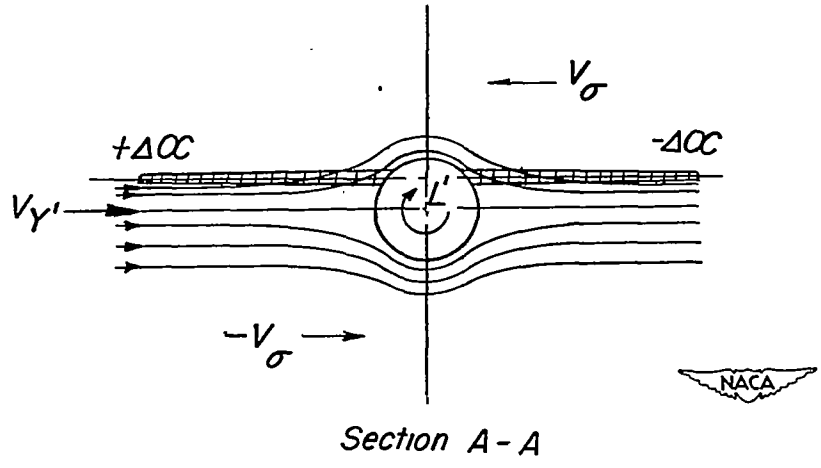

(b) Explanatory sketch for the increase in rolling moment due to yaw by the fuselage interference and for the induced sidewash.

Figure 1.- System of axes used and representation of flow at wing-fuselage juncture and at vertical tail.

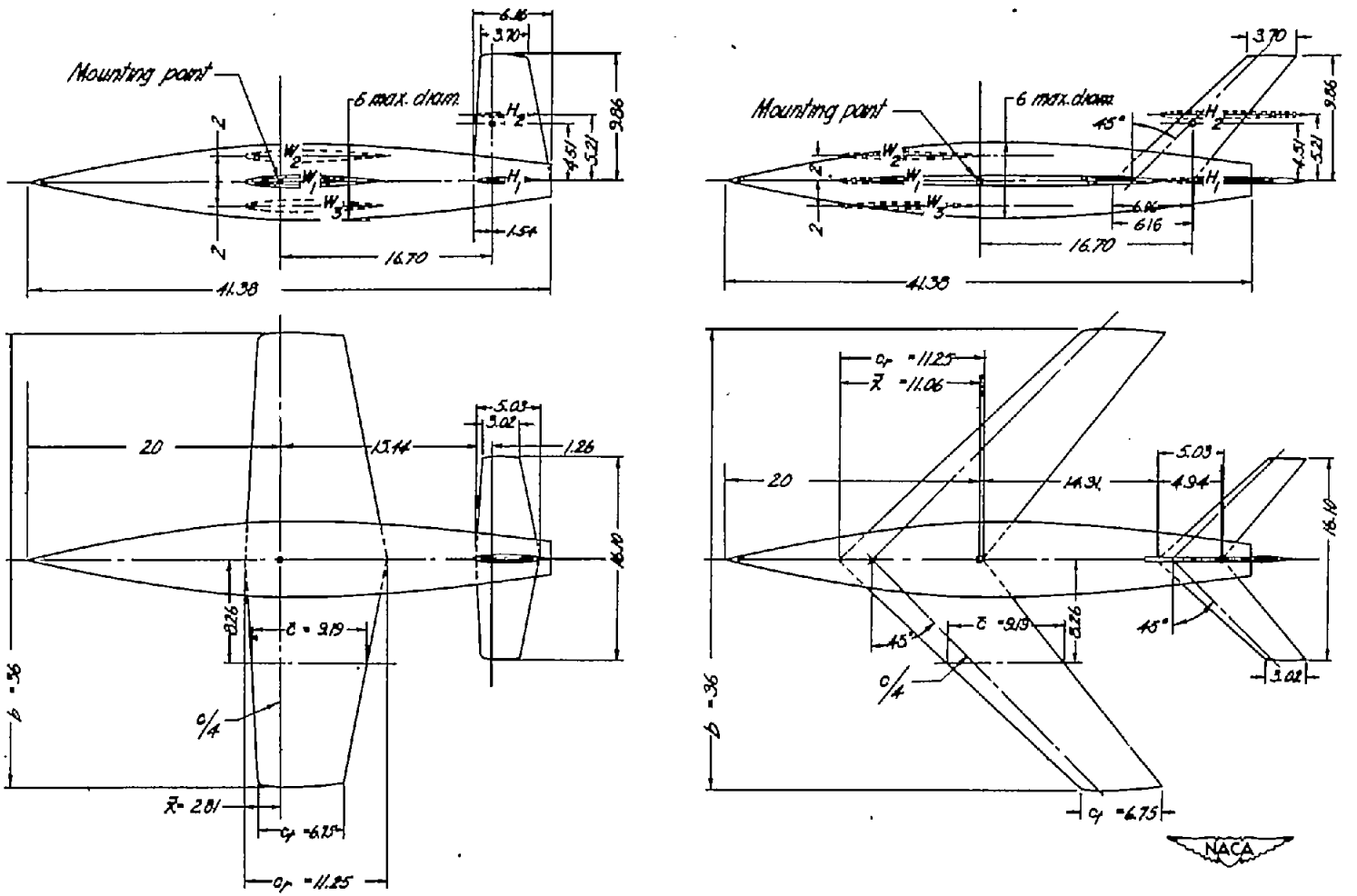

(a) Unswept surfaces.

(b) 45° swept surfaces.

Figure 2.- Dimensions of the complete model. All dimensions are in inches.

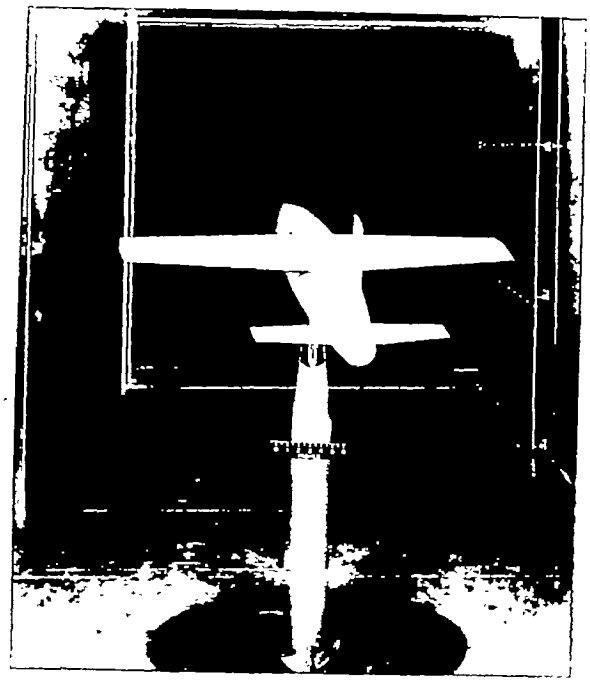

(a) Unswept high-wing configuration; low horizontal tail.

L-68798

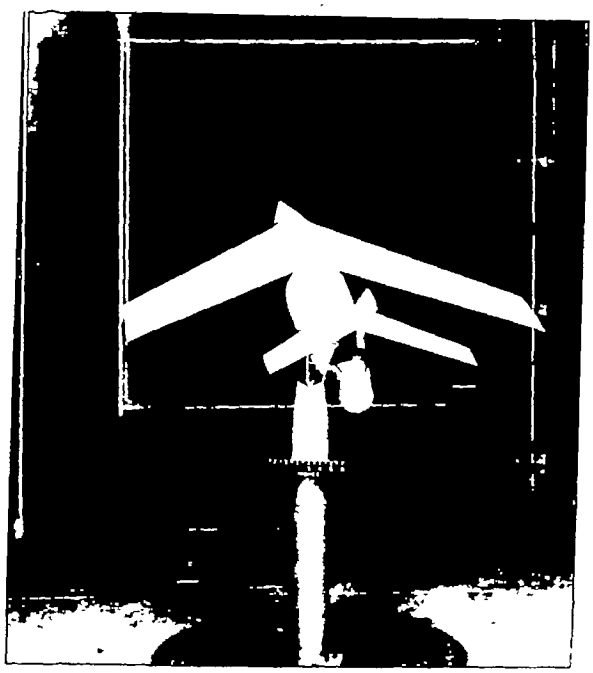

(b) 45° sweptback high-wing configuration; high horizontal tail.

L-68801

Figure 3.- Models mounted in the 6- by 6-foot test section of the Langley stability tunnel.

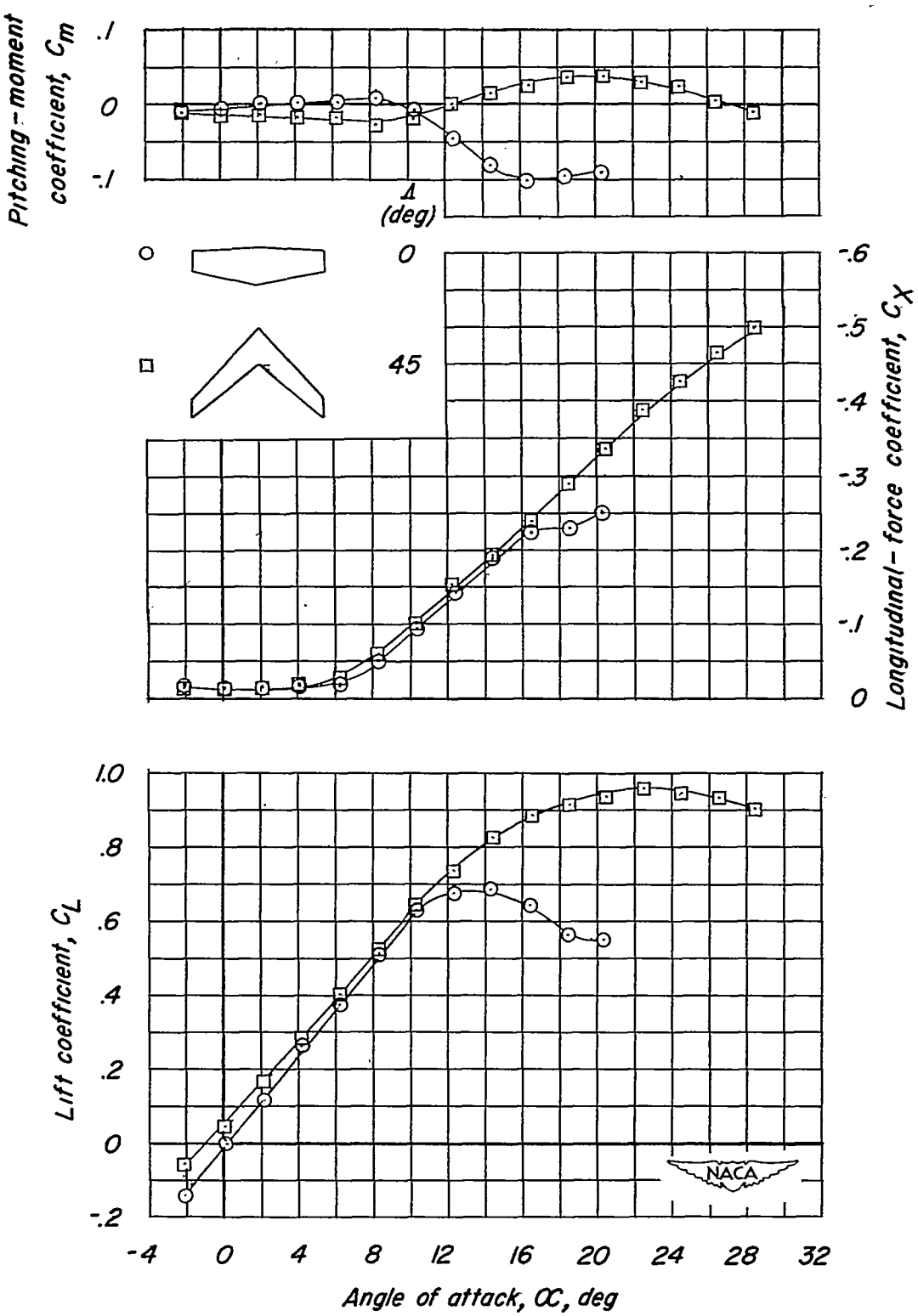

Figure 4.- Aerodynamic characteristics of the unswept and 45° swept-back wings.

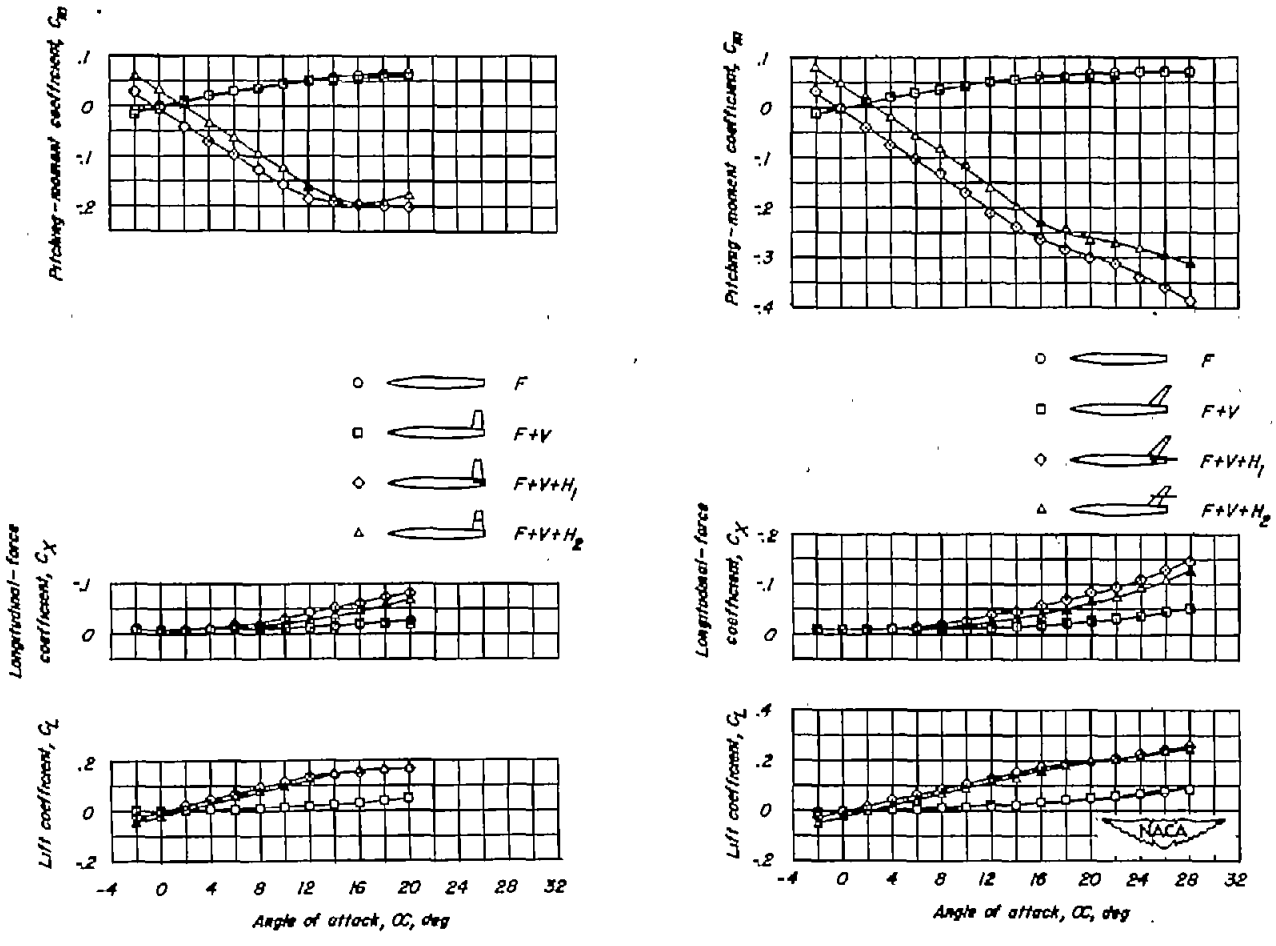

(a) $\Lambda = 0^{\circ}$.

(b) $\Lambda = 45^{\circ}$.

Figure 5.- Aerodynamic characteristics of the fuselage and the fuselage in combination with several unswept and 45° sweptback tail configurations.

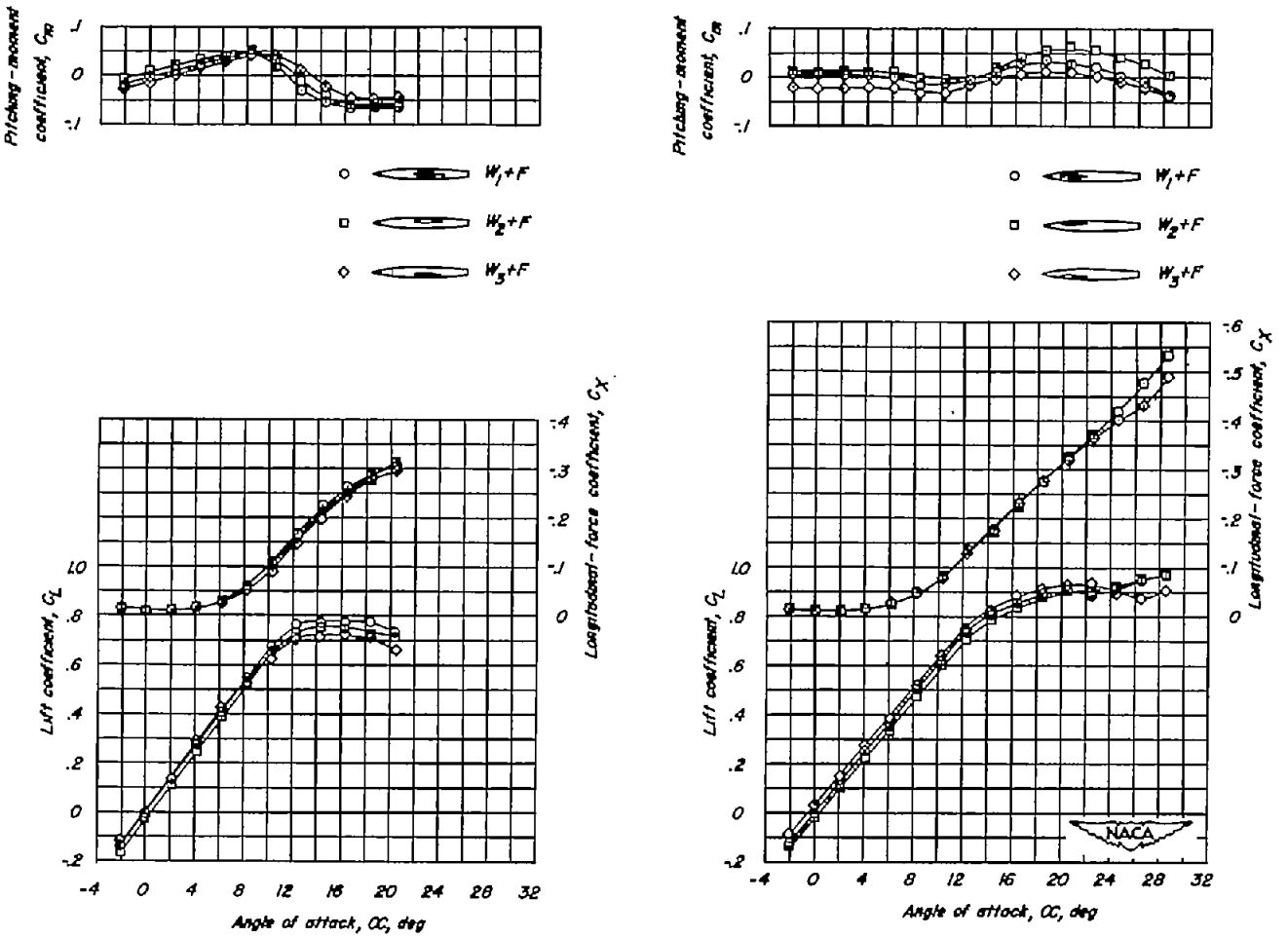

(a) $\Lambda = 0^{\circ}$.

(b) $\Lambda = 45^{\circ}$.

Figure 6.- Effects of wing position on the aerodynamic characteristics of several unswept and 45° sweptback wing-fuselage configurations.

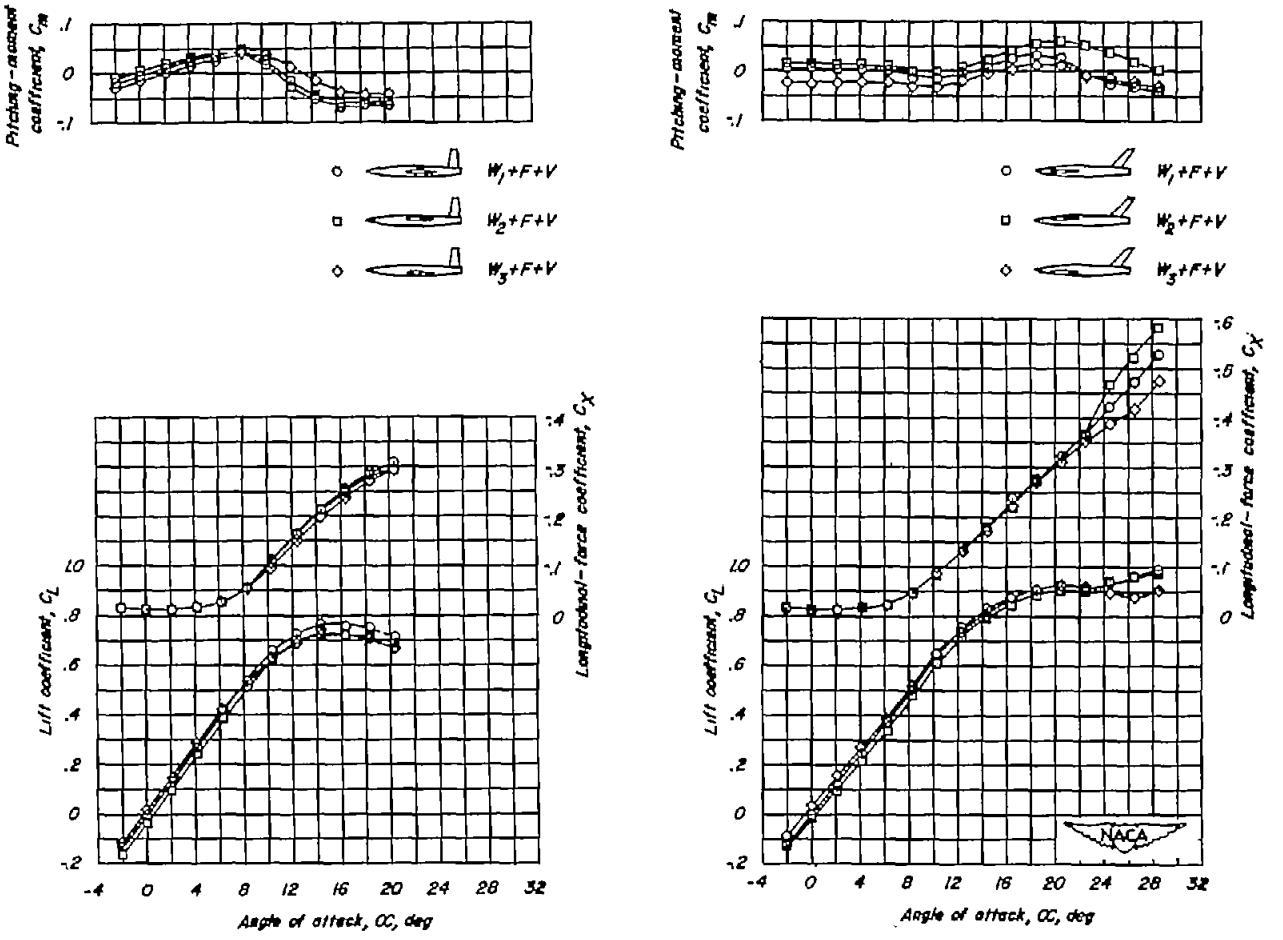

(a) $\Lambda = 0^\circ$.

(b) $\Lambda = 45^\circ$.

Figure 7.- Effects of wing position on the aerodynamic characteristics of several unswept and 45° sweptback wing-fuselage vertical-tail configurations. Horizontal tail off.

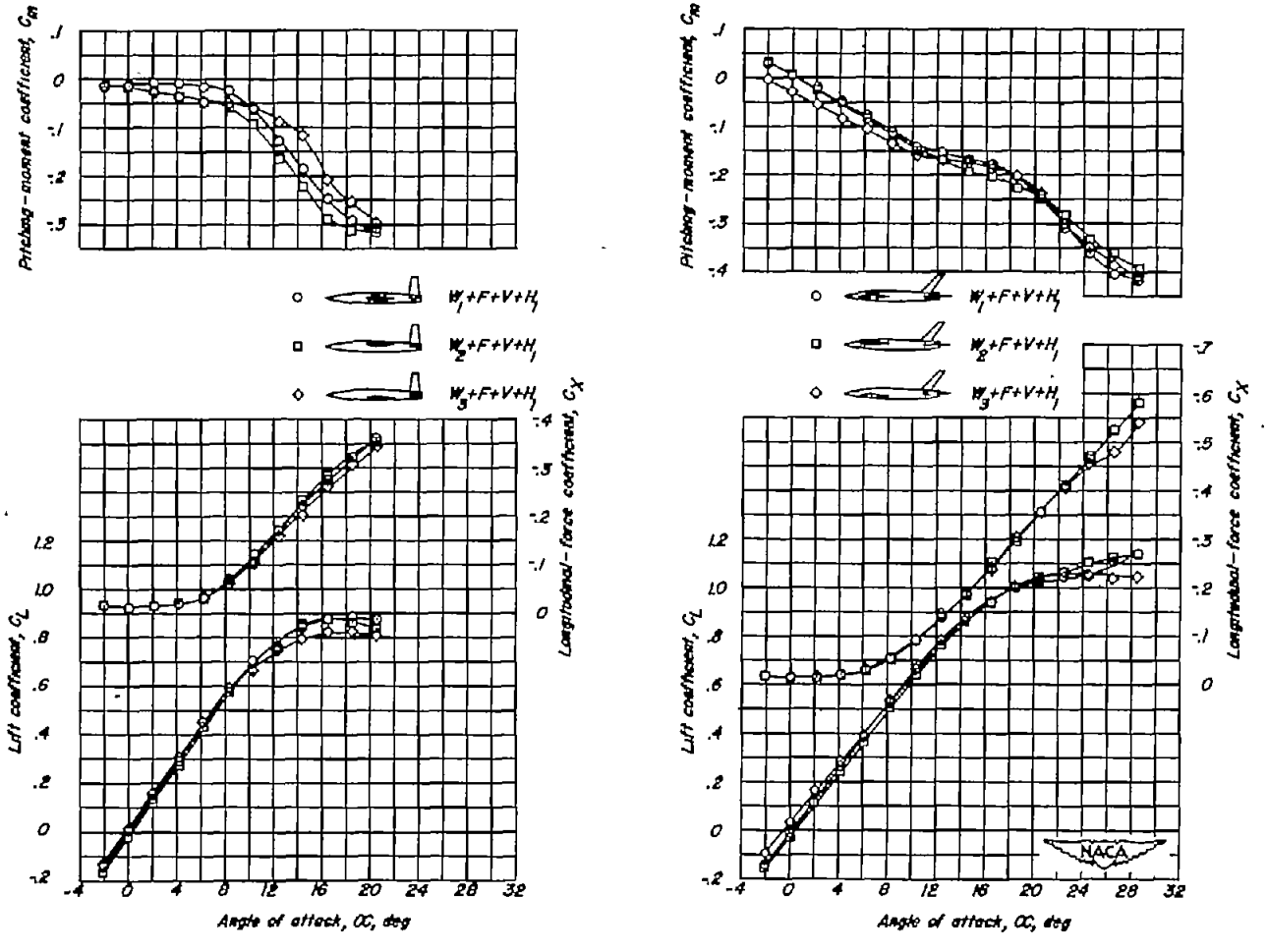

(a) $\Lambda = 0^{\circ}$.

(b) $\Lambda = 45^{\circ}$.

Figure 8.- Effects of wing position on the aerodynamic characteristics of several unswept and 45° sweptback wing-fuselage vertical-tail configurations. Low horizontal tail on.

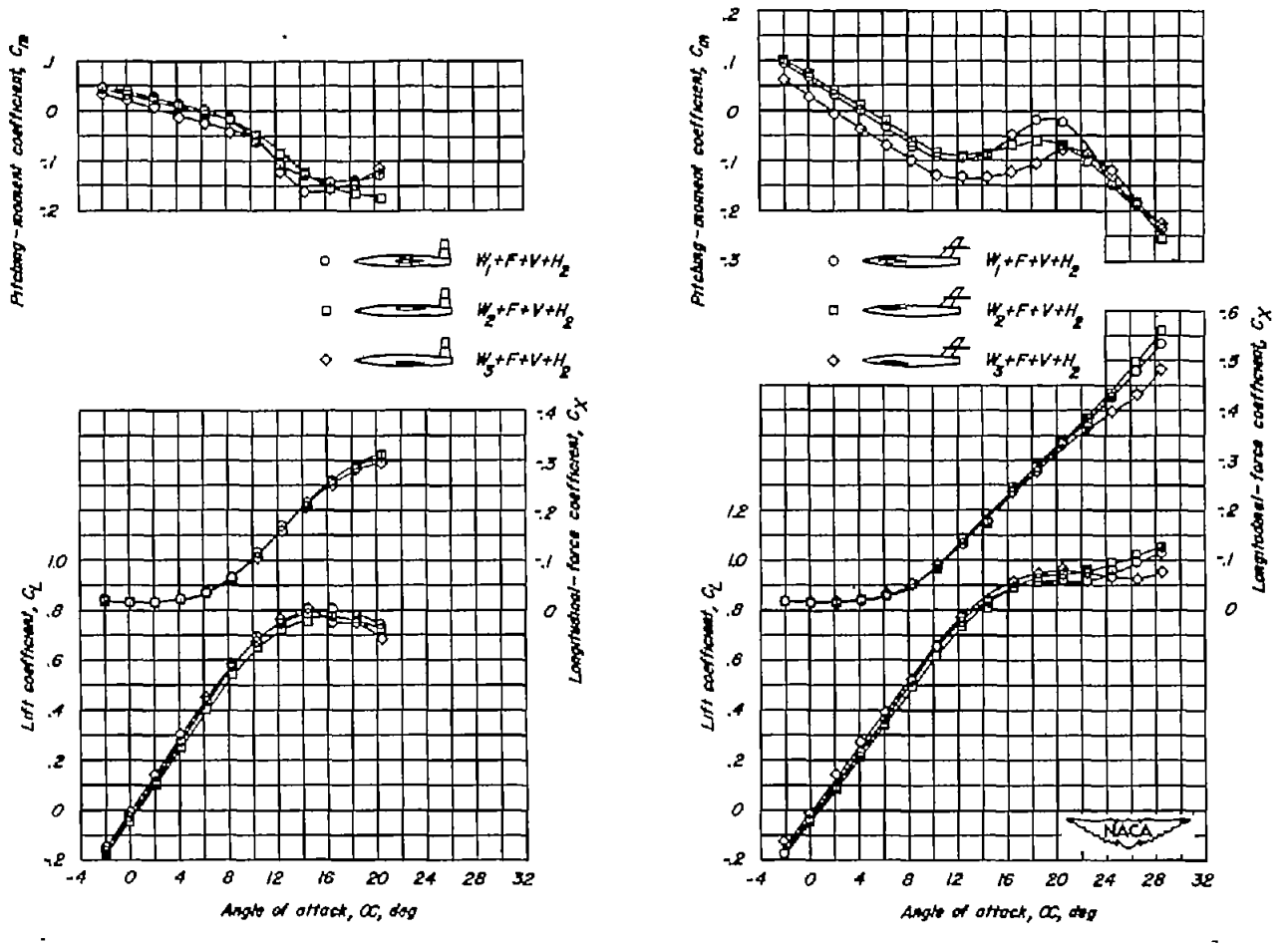

(a) $\Lambda = 0^{\circ}$.

(b) $\Lambda = 45^{\circ}$.

Figure 9.- Effects of wing position on the aerodynamic characteristics of several unswept and 45° sweptback wing-fuselage vertical-tail configurations. High horizontal tail on.

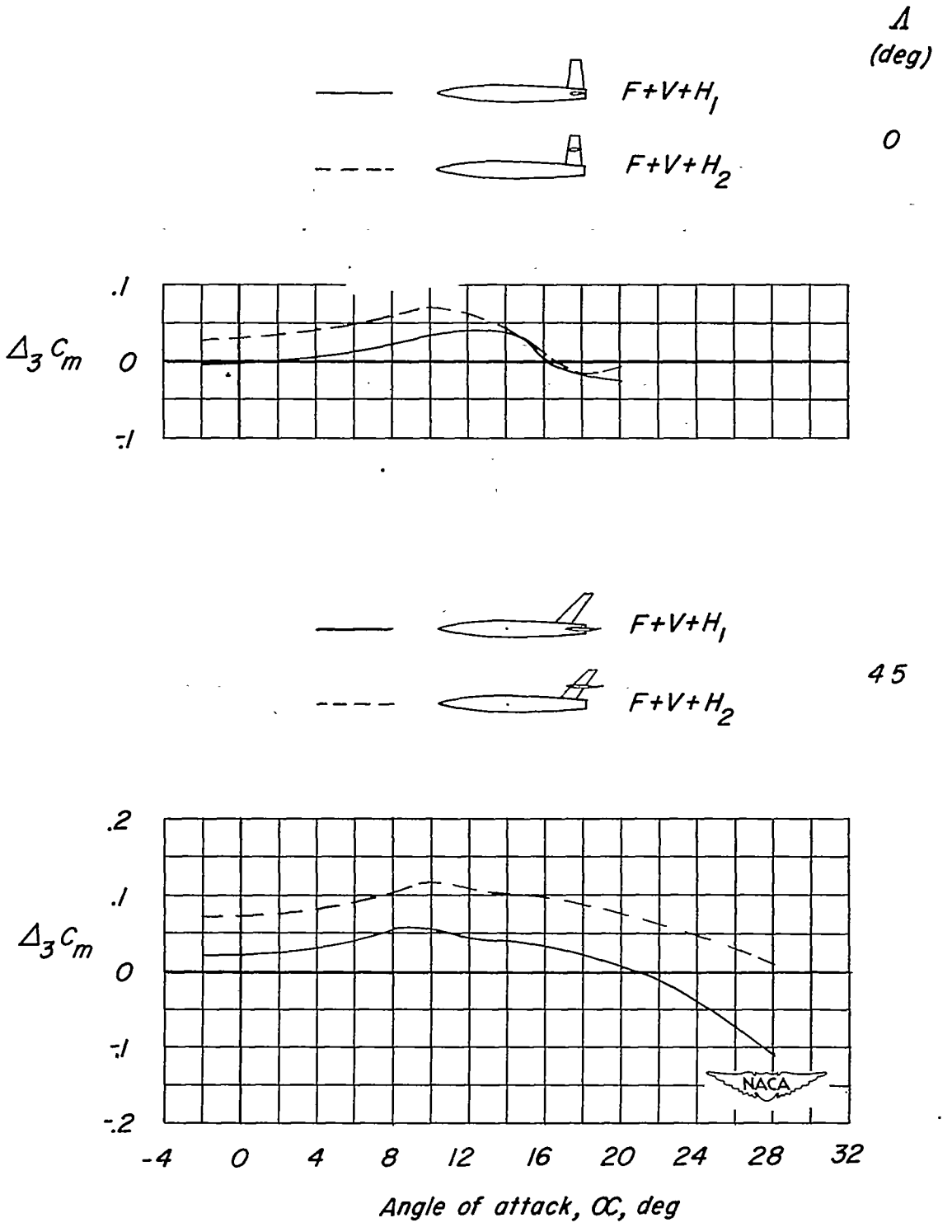

Figure 10.- Variation with angle of attack of the fuselage interference increment $\Delta_3 C_m$ for the unswept and 45° sweptback fuselage-tail configurations.

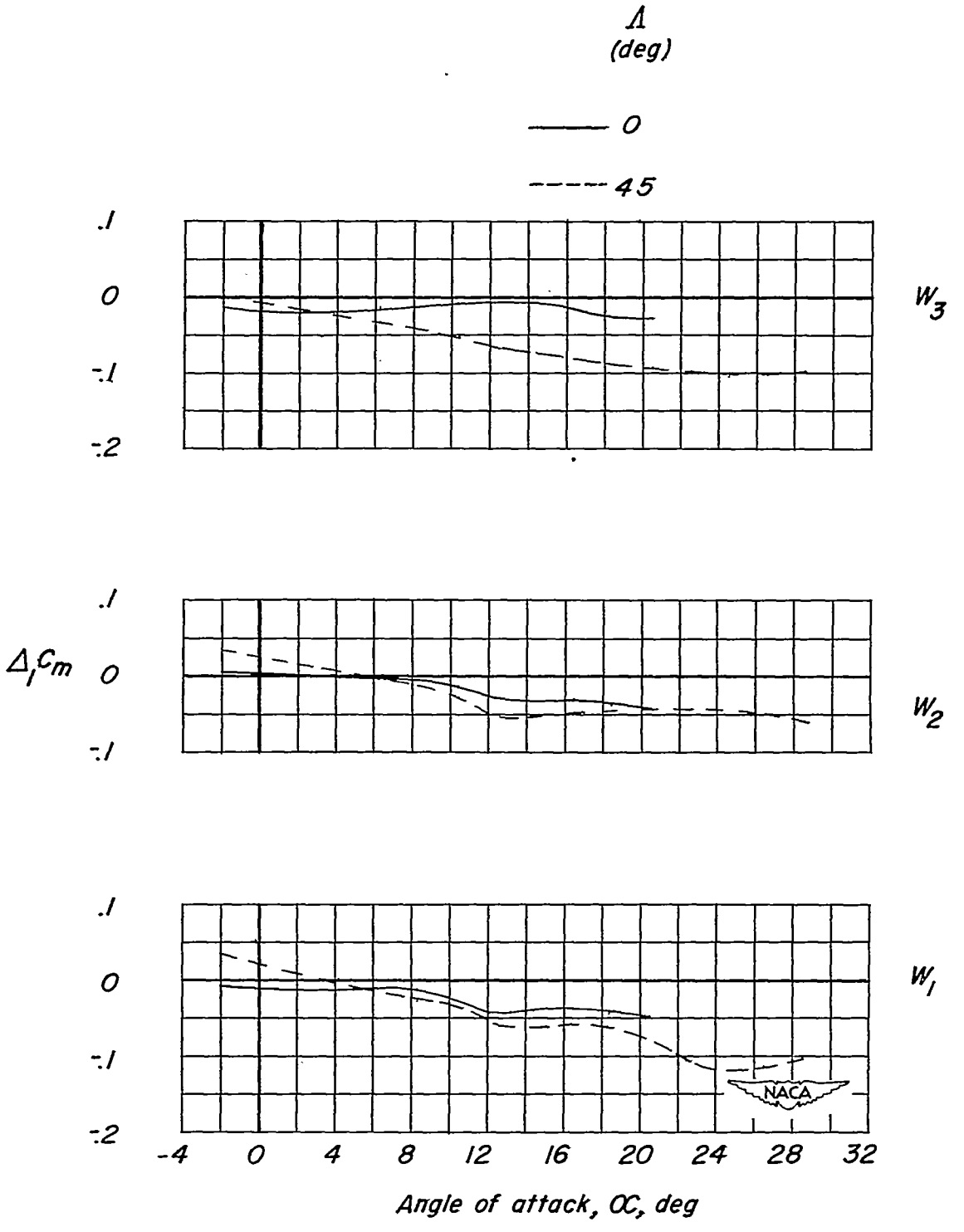

Figure 11.- Variation with angle of attack of the wing-fuselage interference increment $\Delta_1 C_m$ for the unswept and 45° sweptback wing-fuselage configurations.

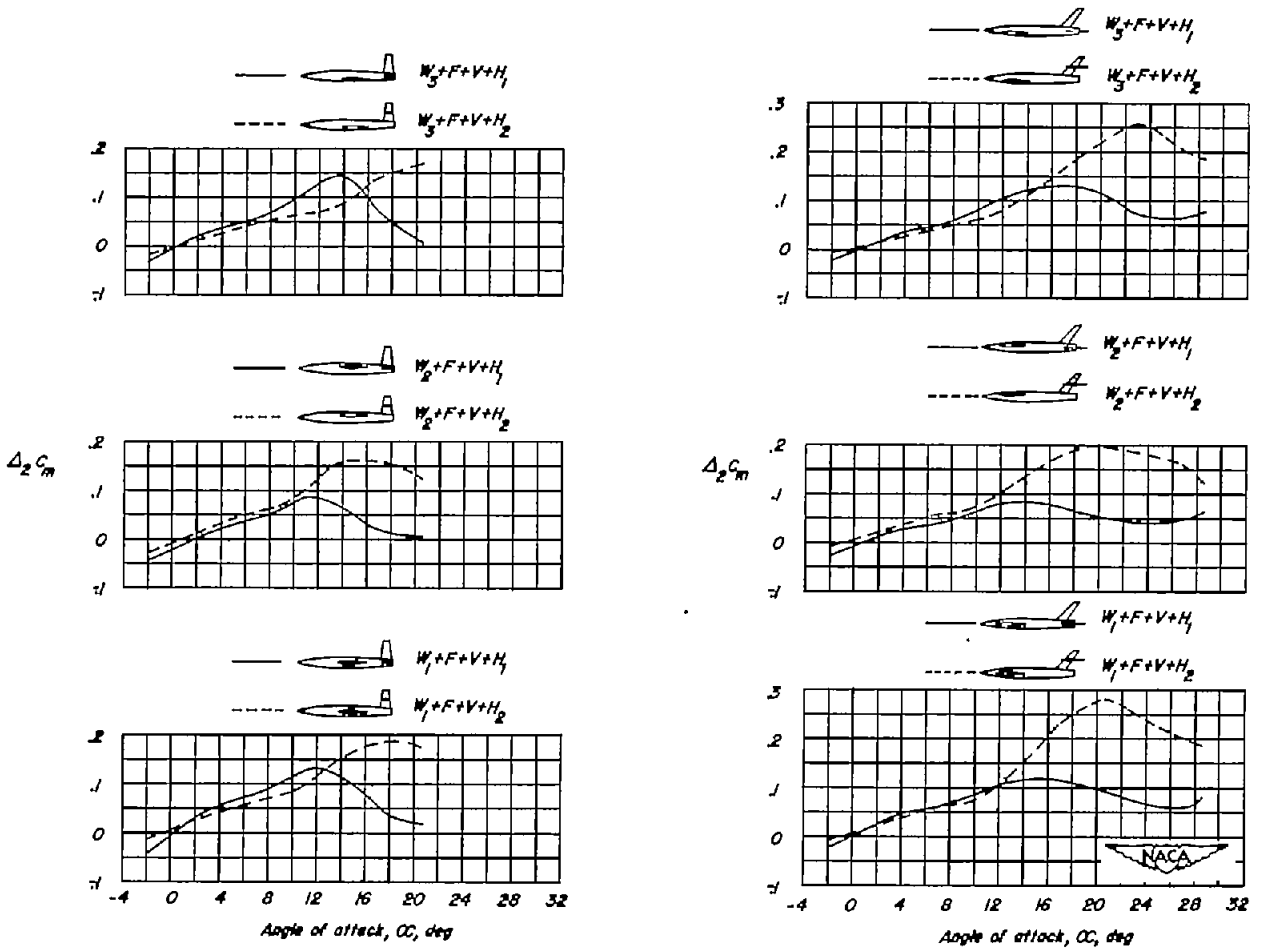

(a) $\Lambda = 0^{\circ}$.

(b) $\Lambda = 45^{\circ}$.

Figure 12.- Variation with angle of attack of the increment $\Delta_2 C_m$ caused by wing-fuselage interference on the horizontal-tail contribution.

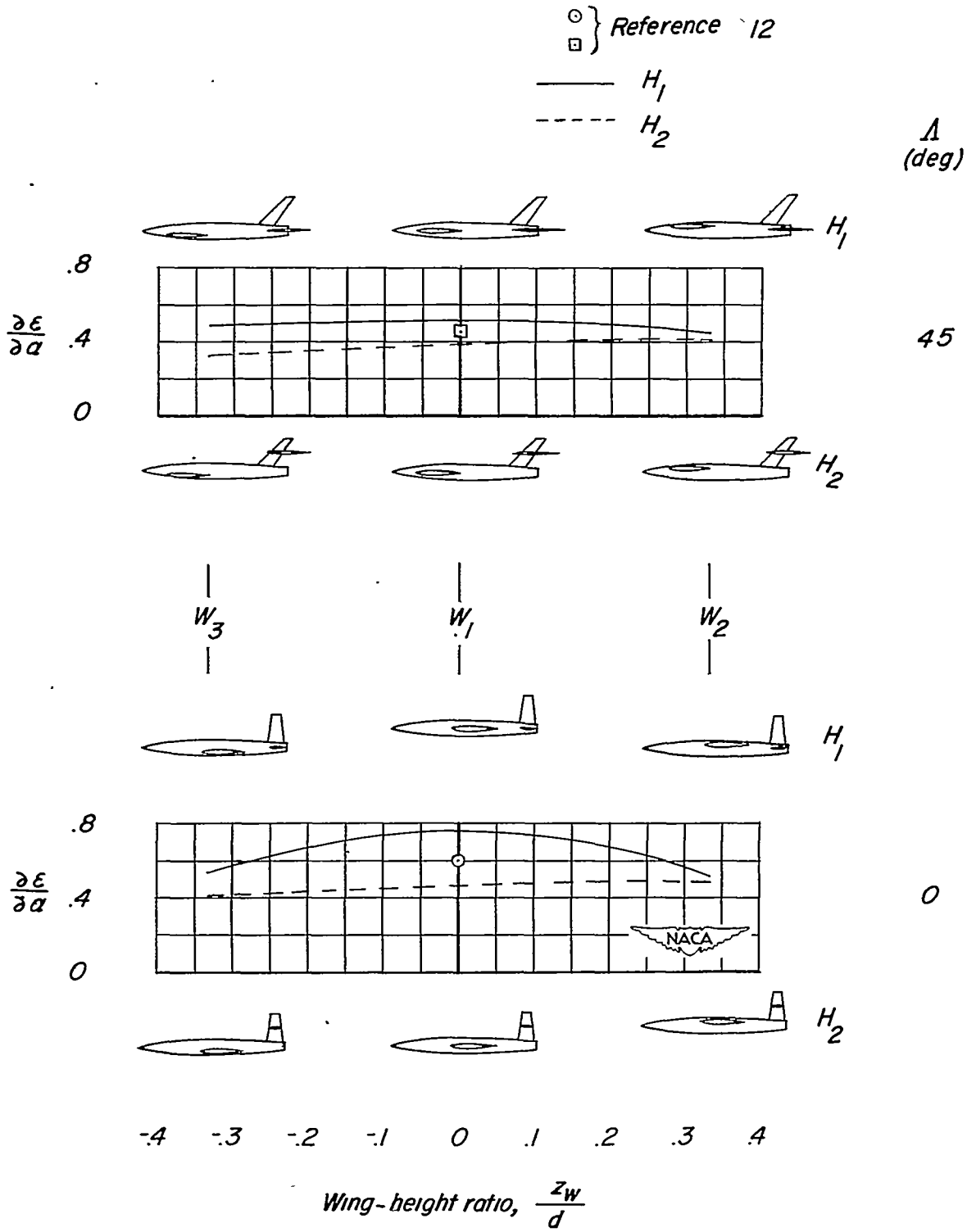

Figure 13.- Variation of the downwash factor $\partial\epsilon/\partial\alpha$ with wing-height ratio for the unswept and 45° sweptback tails. $\alpha = 0^{\circ}$.

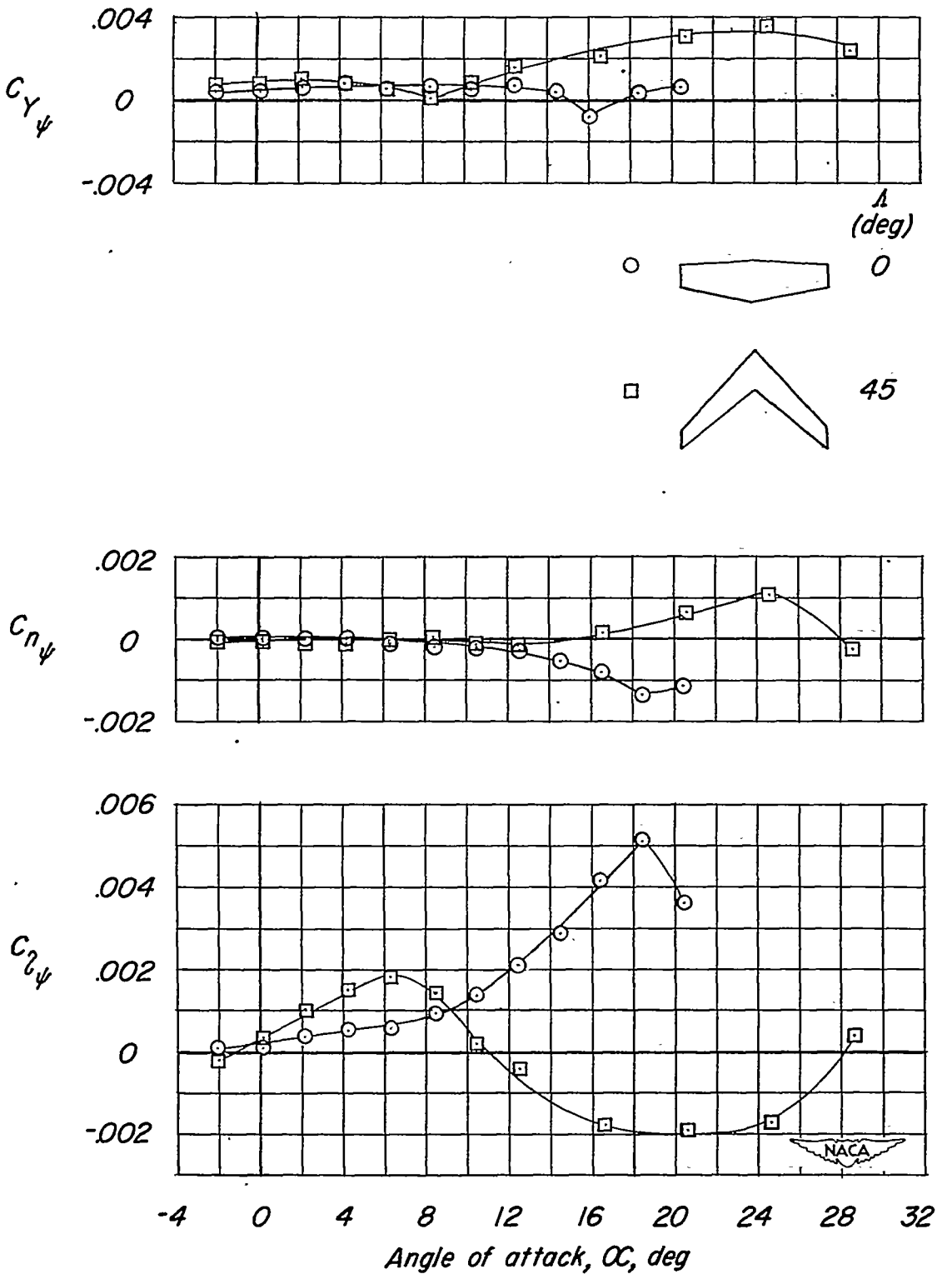

Figure 14.- Static lateral stability characteristics of the unswept and 45° sweptback wings.

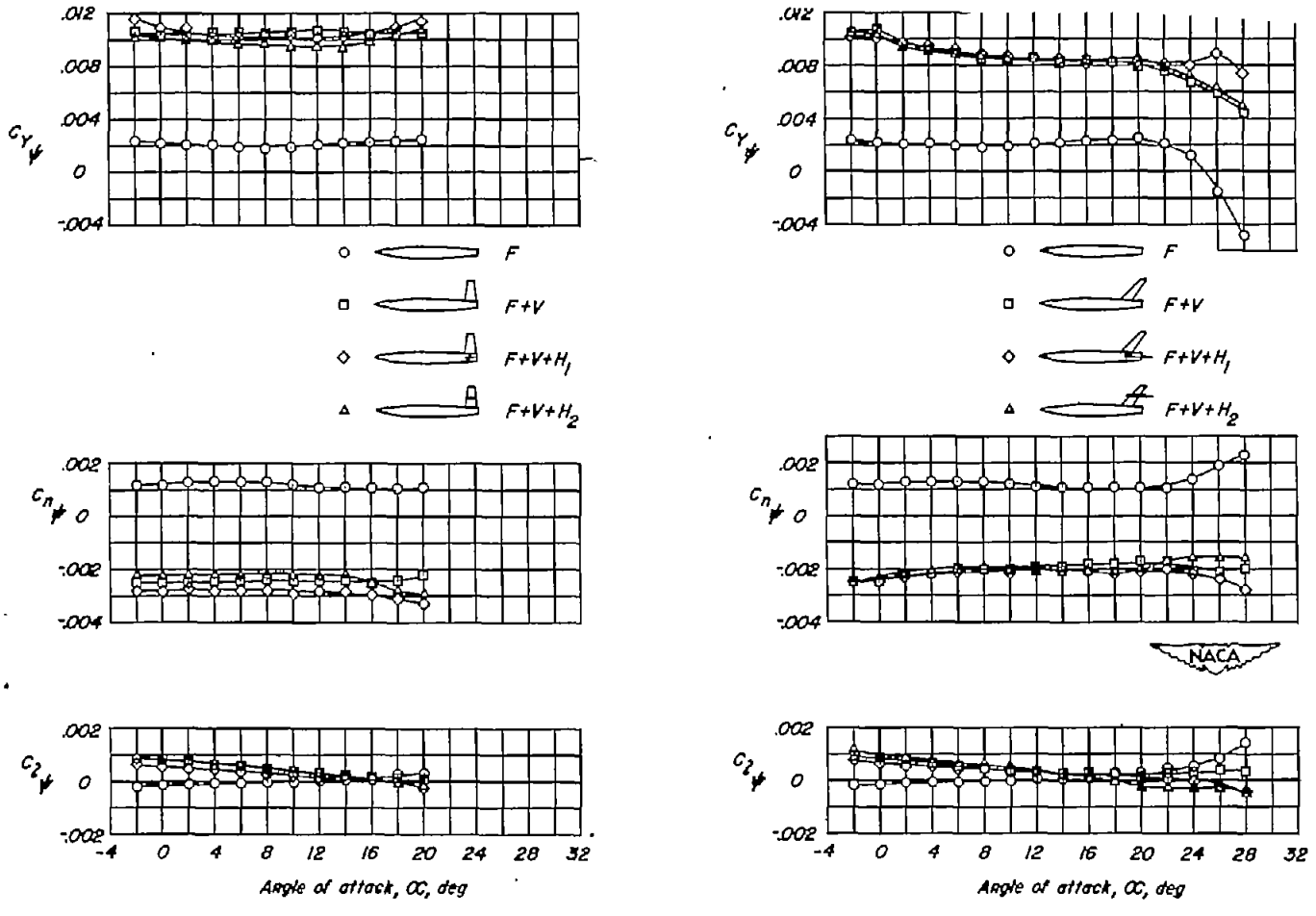

(a) $\Lambda = 0^{\circ}$.

(b) $\Lambda = 45^{\circ}$.

Figure 15.- Static lateral stability characteristics of the fuselage and the fuselage in combination with several unswept and 45° sweptback tail configurations.

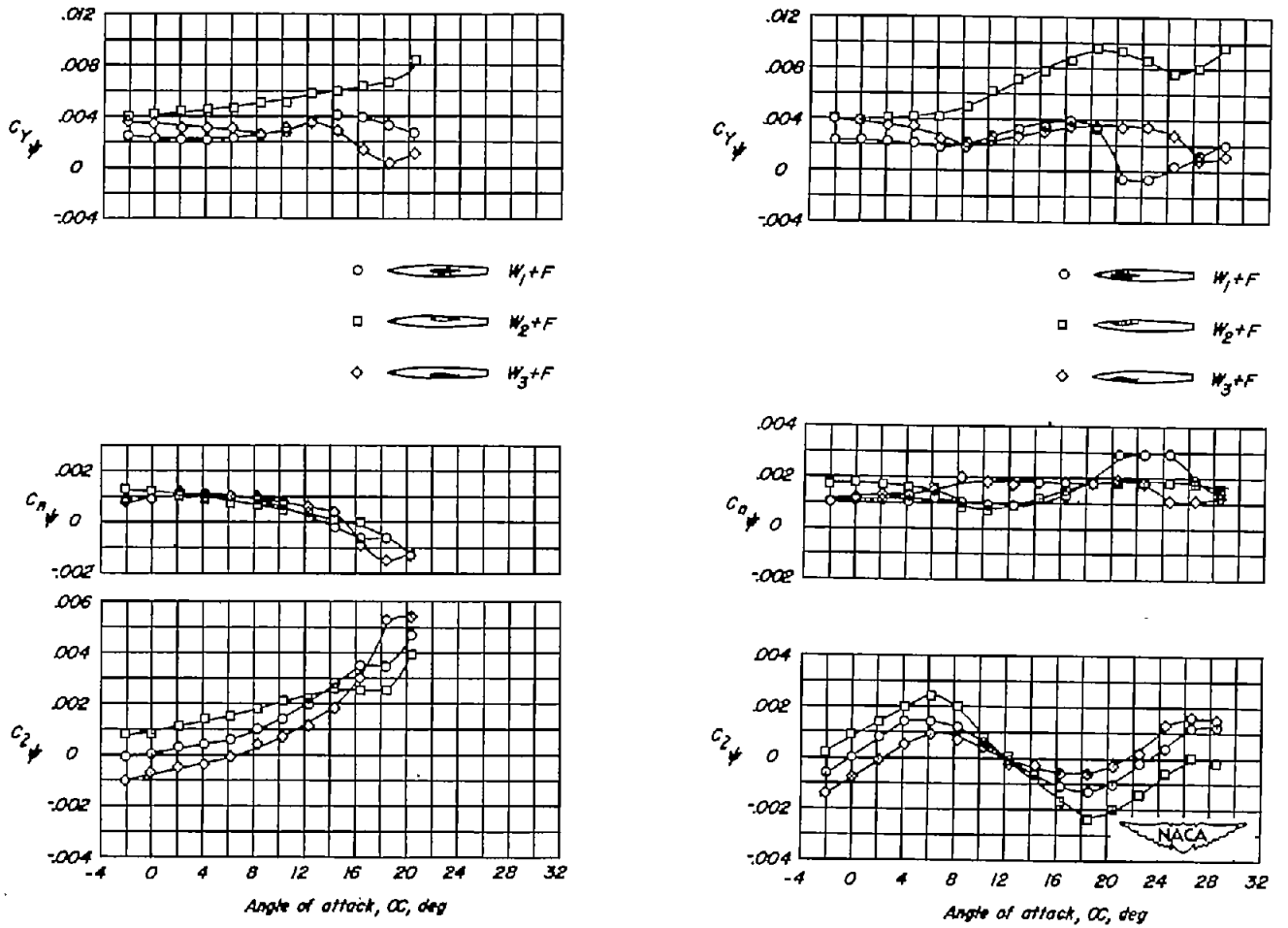

(a) $\Lambda = 0^{\circ}$.

(b) $\Lambda = 45^{\circ}$.

Figure 16.- Effects of wing position on the static lateral stability characteristics of several unswept and 45° sweptback wing-fuselage configurations.

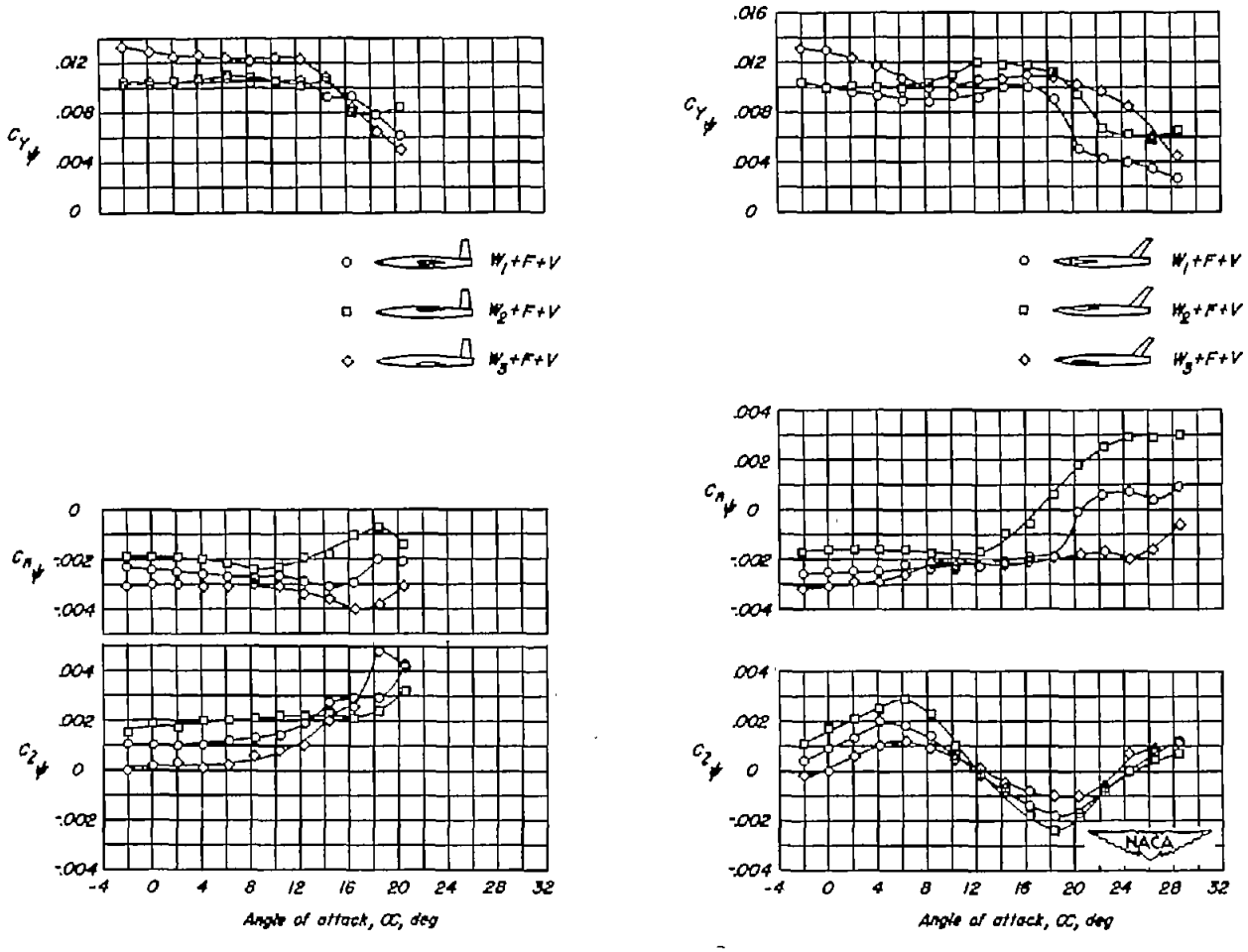

(a) $\Lambda = 0^\circ$.

(b) $\Lambda = 45^\circ$.

Figure 17.- Effects of wing position on the static lateral stability characteristics of several unswept and 45° sweptback wing-fuselage vertical-tail configurations. Horizontal tail off.

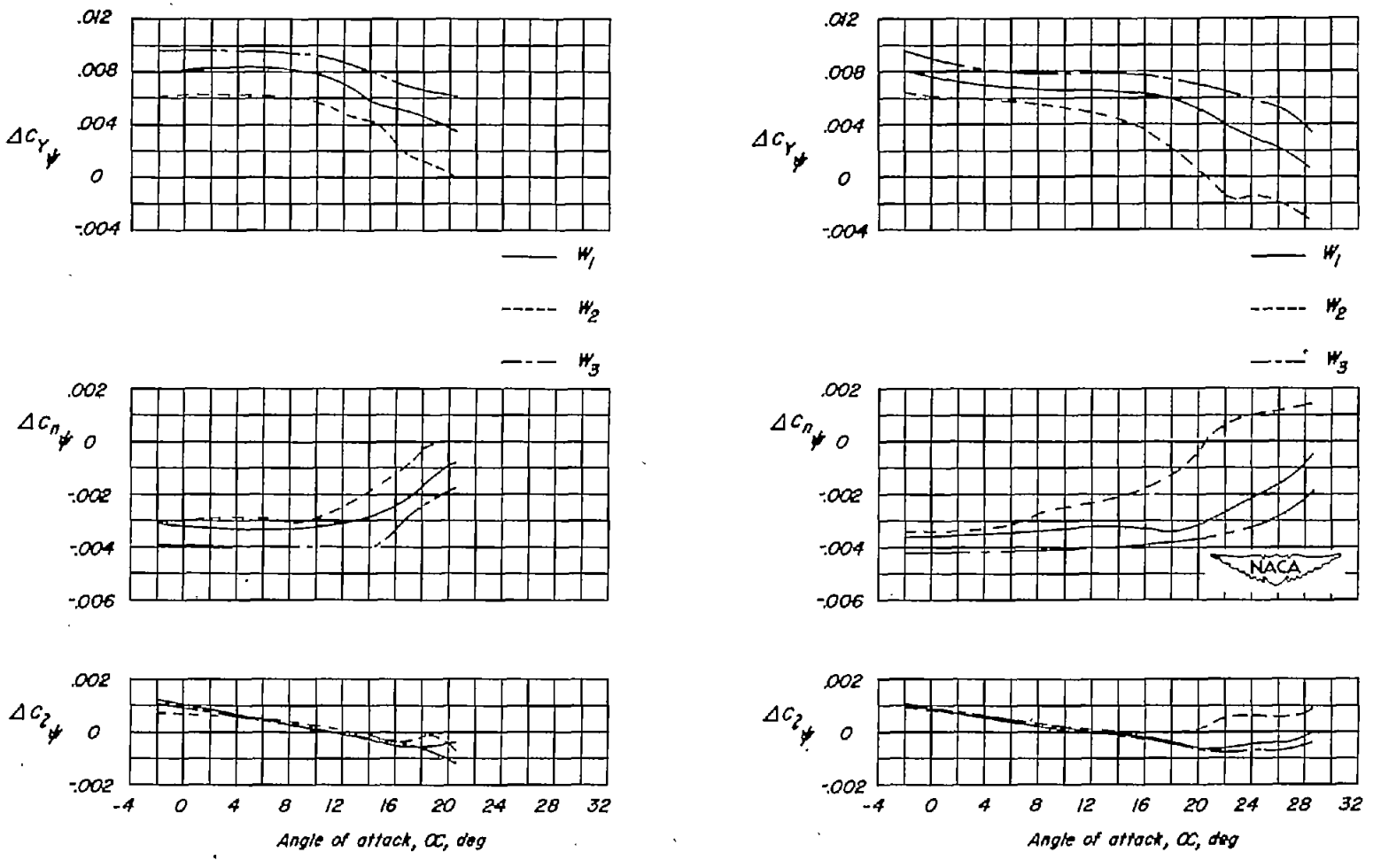

(a) $\Lambda = 0^\circ$.

(b) $\Lambda = 45^\circ$.

Figure 18.- Effects of wing position on the contribution of the vertical tail to the derivatives C_{Y_ψ}, C_{n_ψ}, and C_{l_ψ}. Horizontal tail off.

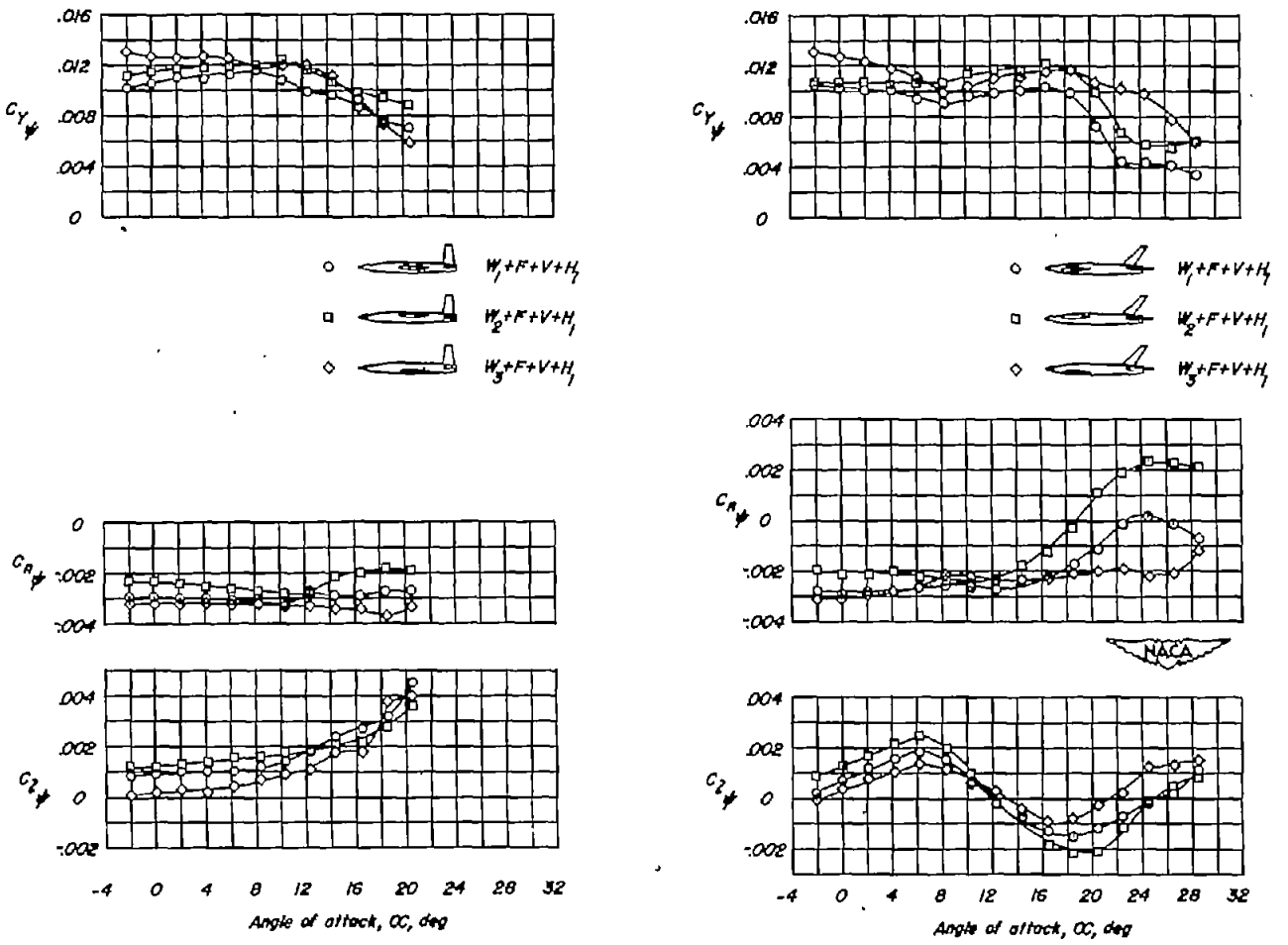

(a) $\Lambda = 0^\circ$.

(b) $\Lambda = 45^\circ$.

Figure 19.- Effects of wing position on the static lateral stability characteristics of several unswept and 45° sweptback wing-fuselage vertical-tail configurations. Low horizontal tail on.

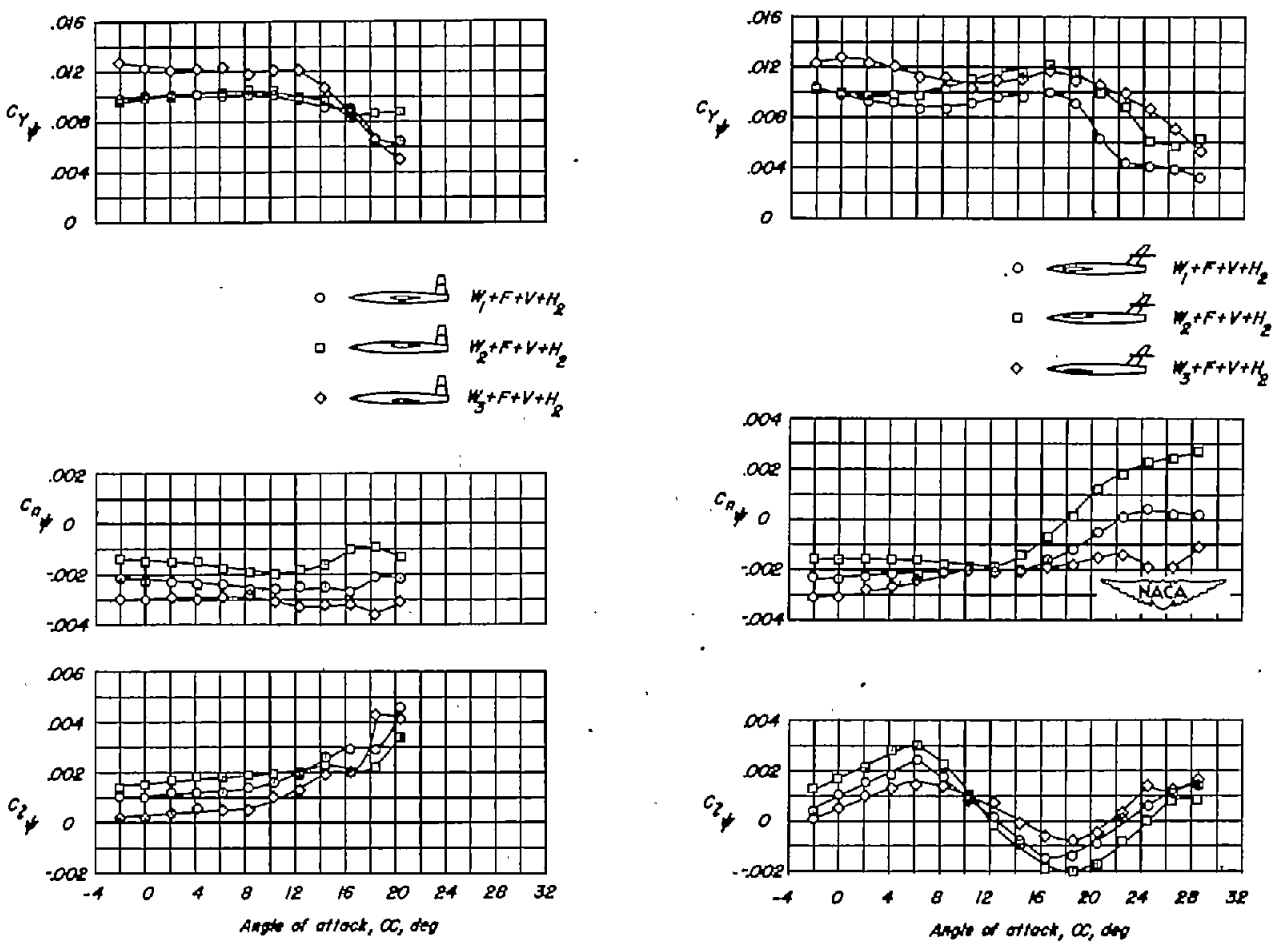

(a) $\Lambda = 0^\circ$.

(b) $\Lambda = 45^\circ$.

Figure 20.- Effects of wing position on the static lateral stability characteristics of several unswept and 45° sweptback wing-fuselage vertical-tail configurations. High horizontal tail on.

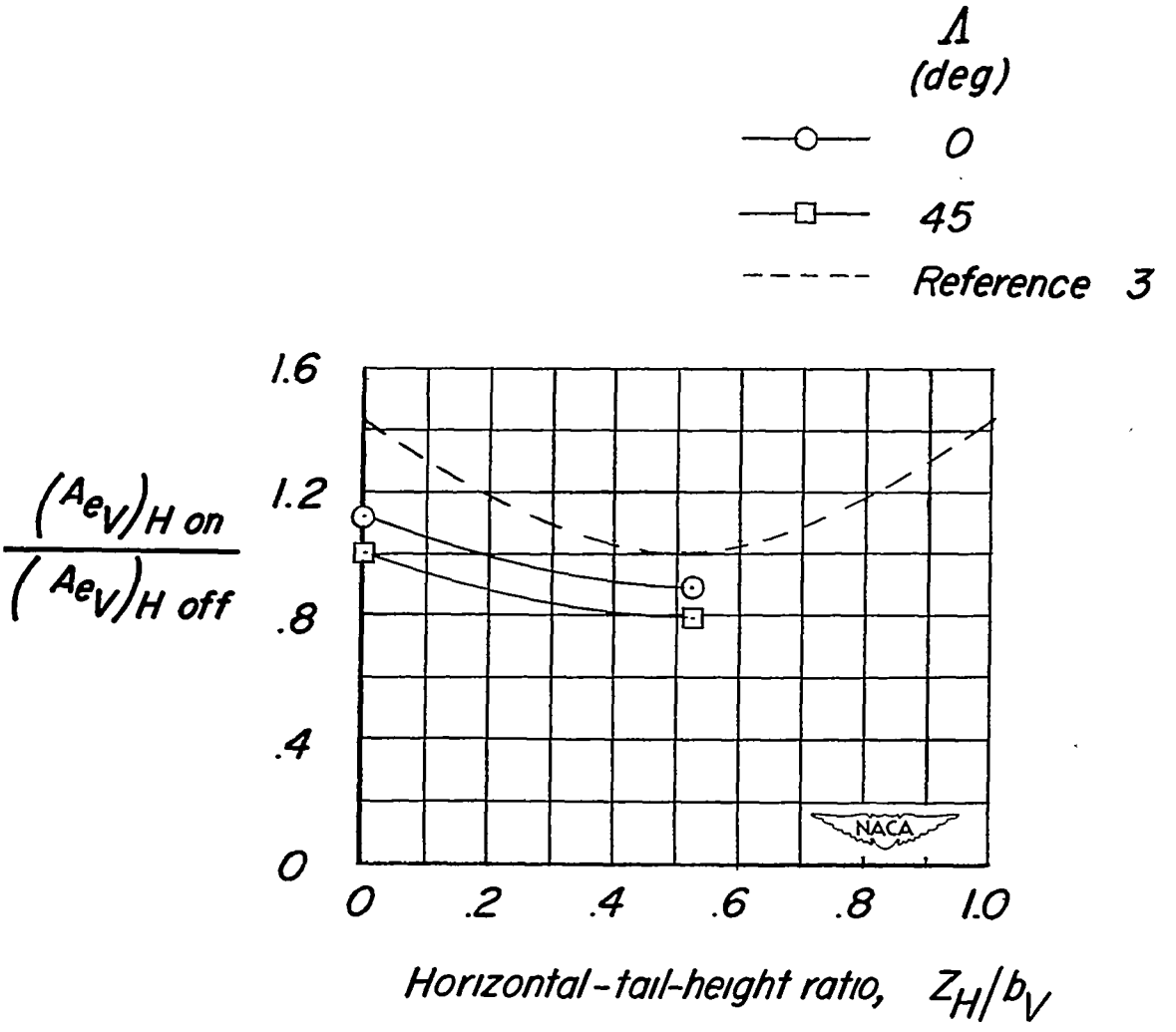

Figure 21.- Variation of the ratio $\frac{(A_{e_V})_{H\ on}}{(A_{e_V})_{H\ off}}$ with horizontal-tail-height ratio Z_H/b_V for the unswept and 45° sweptback tails. $\alpha_H = 0^\circ$; wing off.

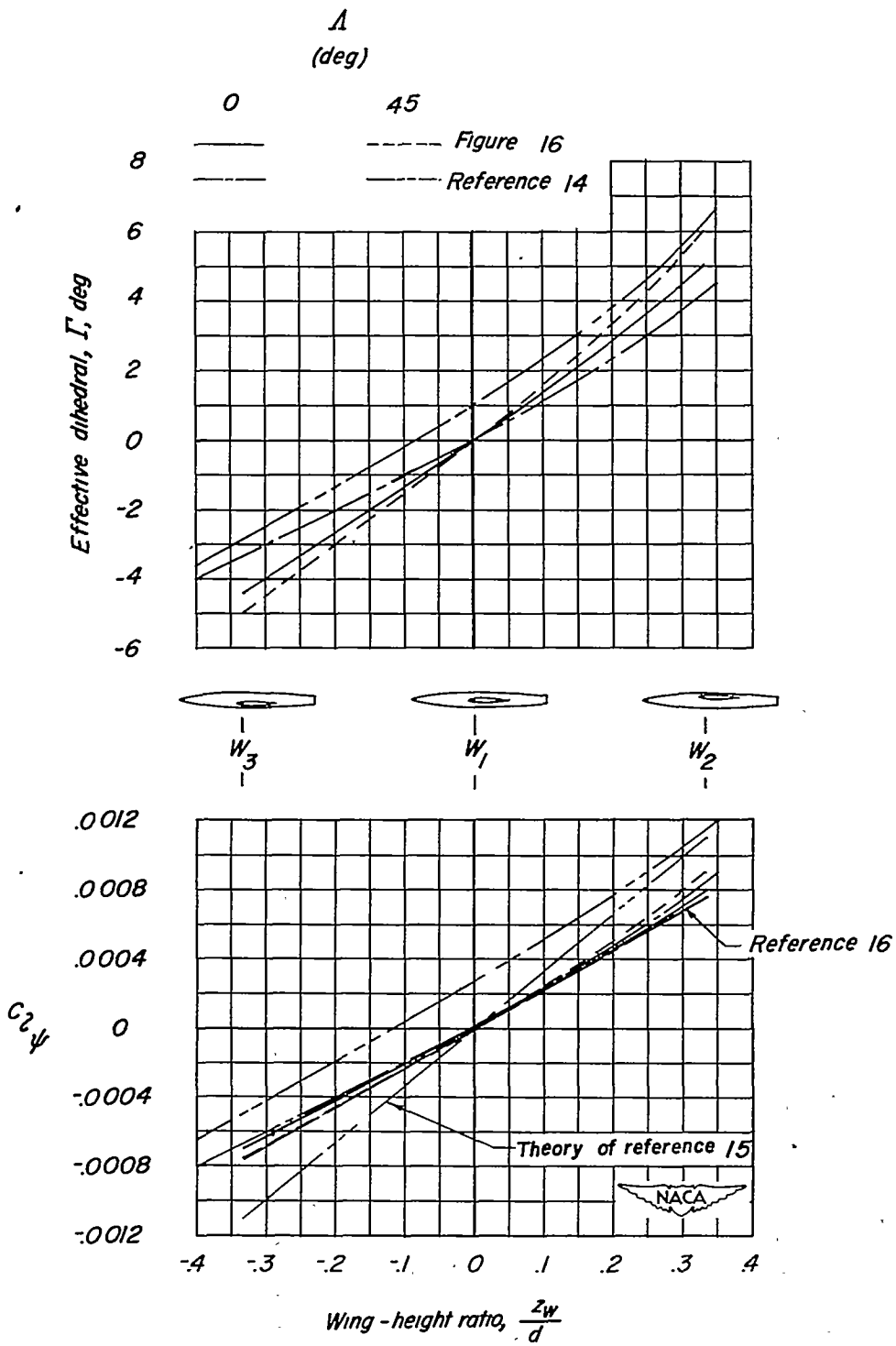

Figure 22.- Variation with wing-height ratio of the increments in C_{l_ψ} and effective dihedral due to wing-fuselage interference for unswept and 45° sweptback wing-fuselage configurations. $\alpha = 0^\circ$.

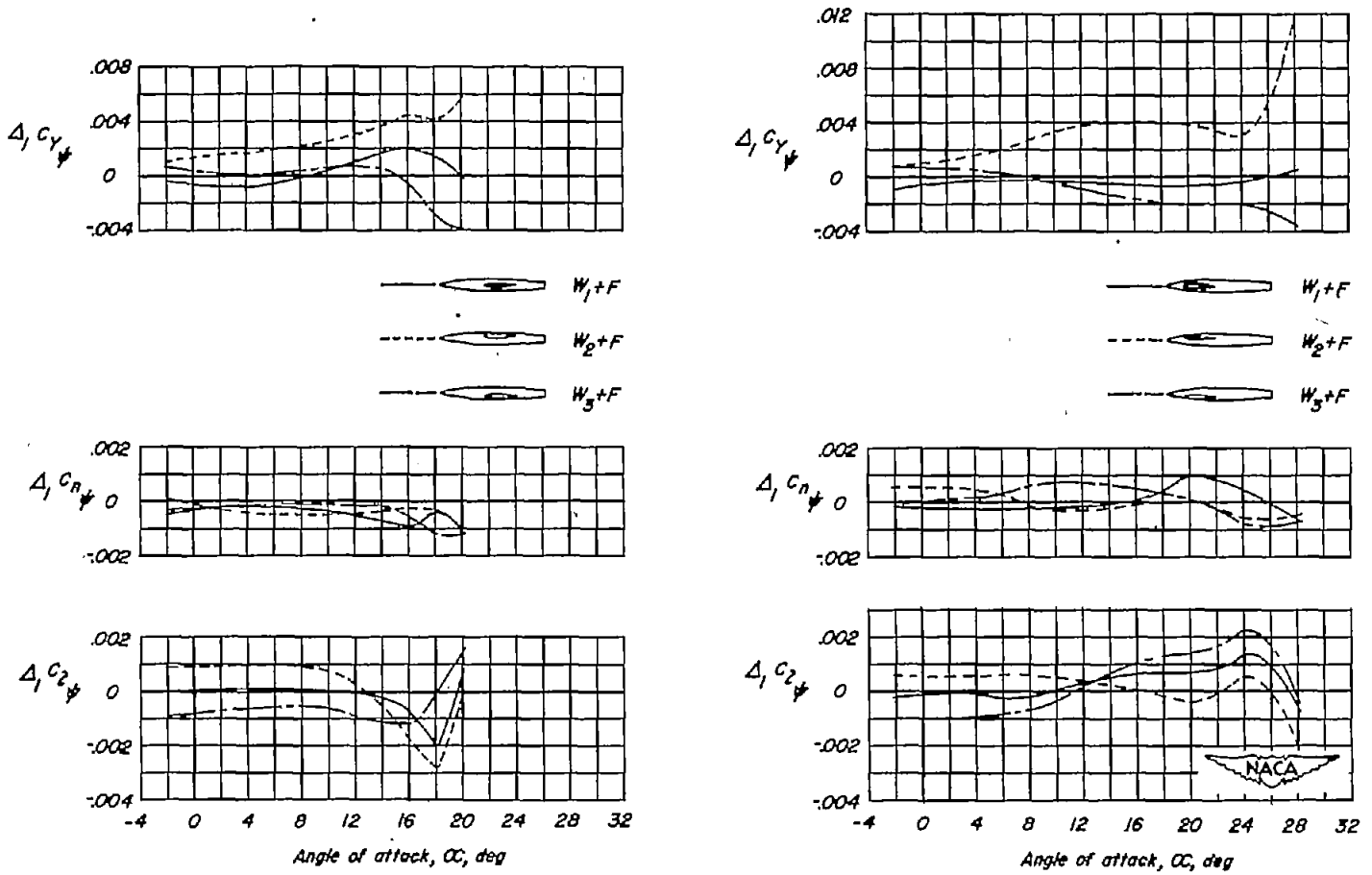

(a) $\Lambda = 0^\circ$.

(b) $\Lambda = 45^\circ$.

Figure 23.- Effects of wing position on the wing-fuselage increments $\Delta_1 C_{Y_\psi}$, $\Delta_1 C_{n_\psi}$, and $\Delta_1 C_{l_\psi}$ for the unswept and 45° swept-back wing configurations.

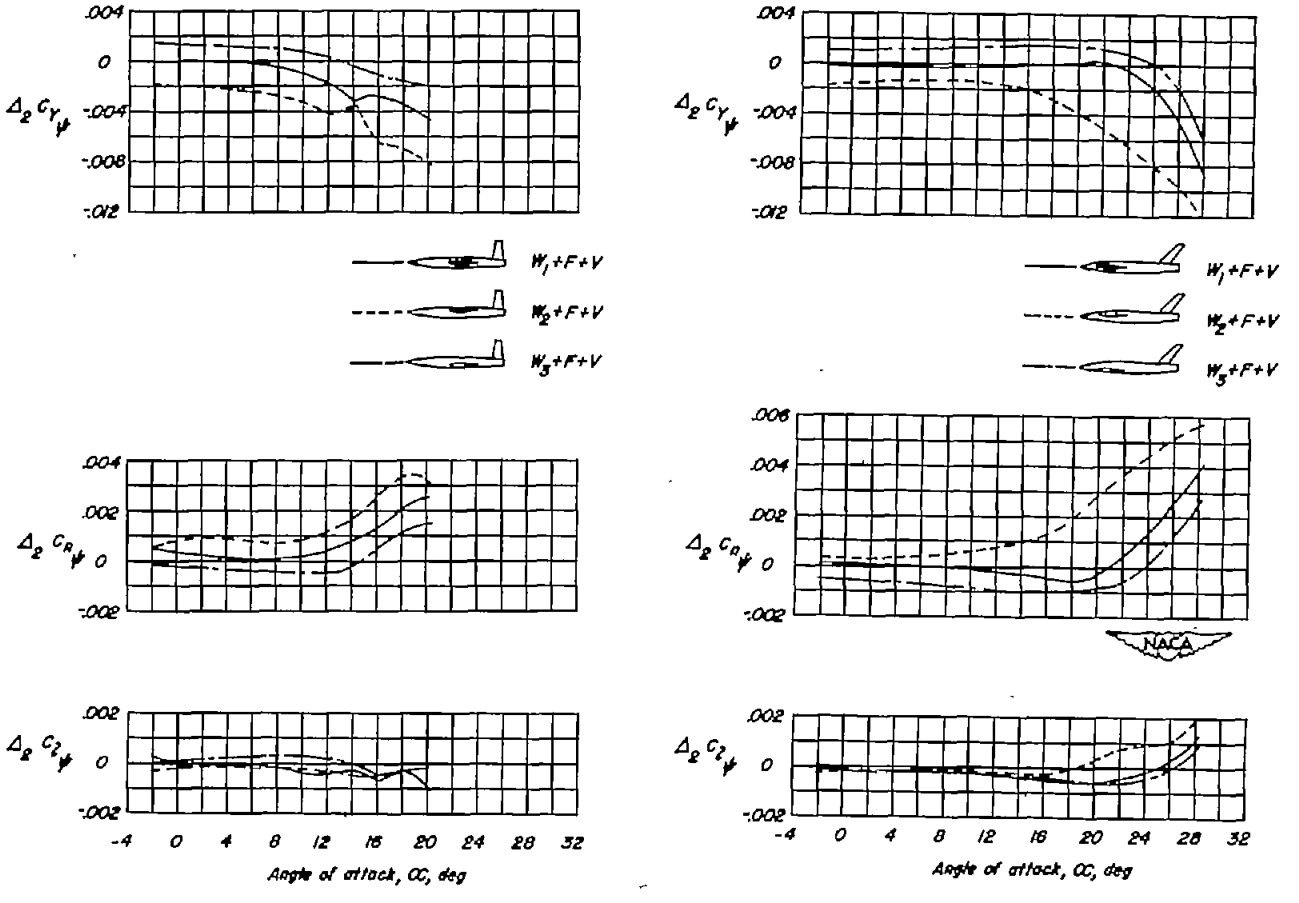

(a) $\Lambda = 0^\circ$.

(b) $\Lambda = 45^\circ$.

Figure 24.- Effects of wing position on the increments caused by wing-fuselage interference on the vertical-tail contributions $\Delta_2 C_{Y_\psi}$, $\Delta_2 C_{n_\psi}$, and $\Delta_2 C_{l_\psi}$. Horizontal tail off.

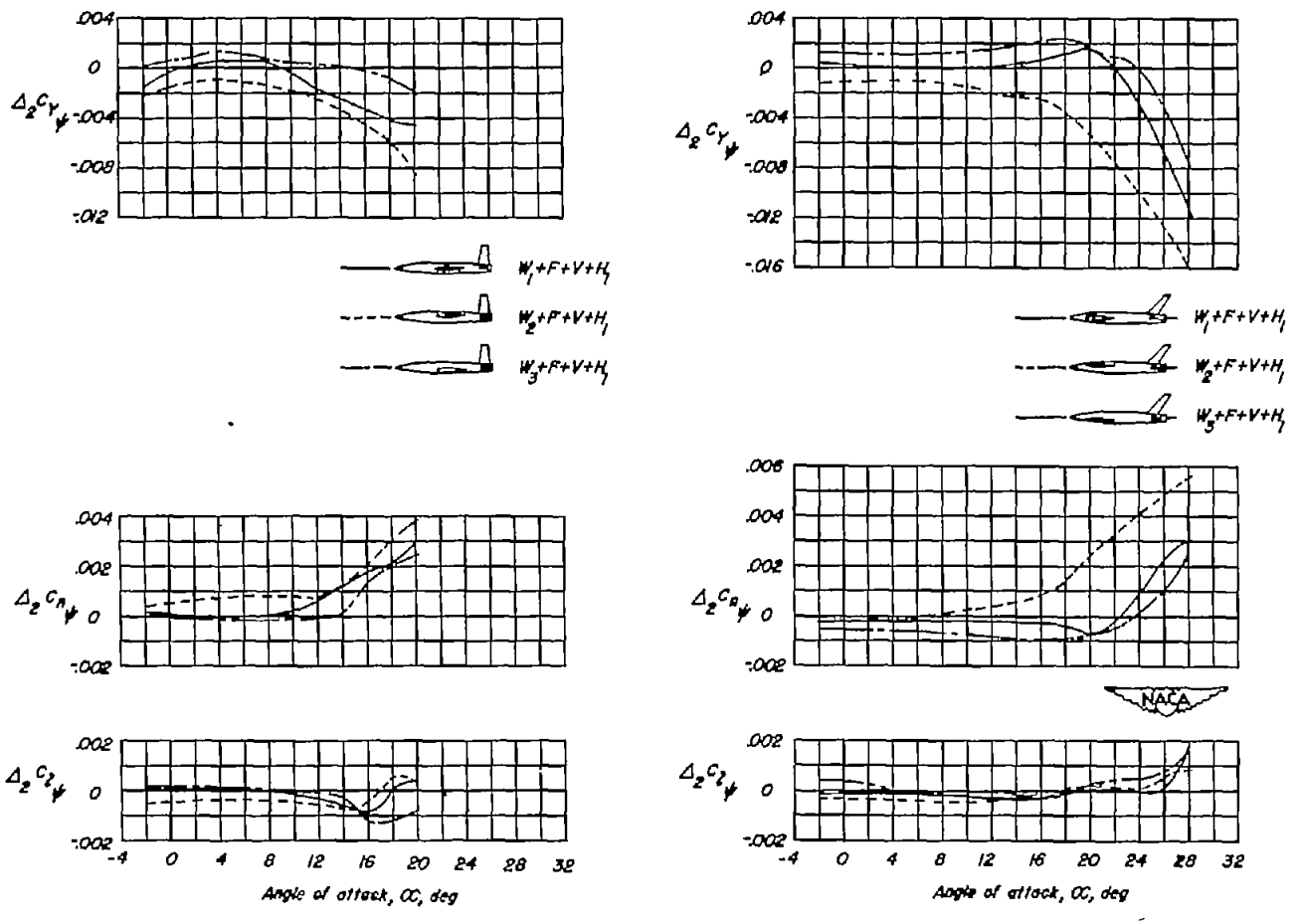

(a) $\Lambda = 0^\circ$.

(b) $\Lambda = 45^\circ$.

Figure 25.- Effects of wing position on the increments caused by wing-fuselage interference on the vertical-tail contributions $\Delta_2 C_{Y_\psi}$, $\Delta_2 C_{n_\psi}$, and $\Delta_2 C_{l_\psi}$. Low horizontal tail on.

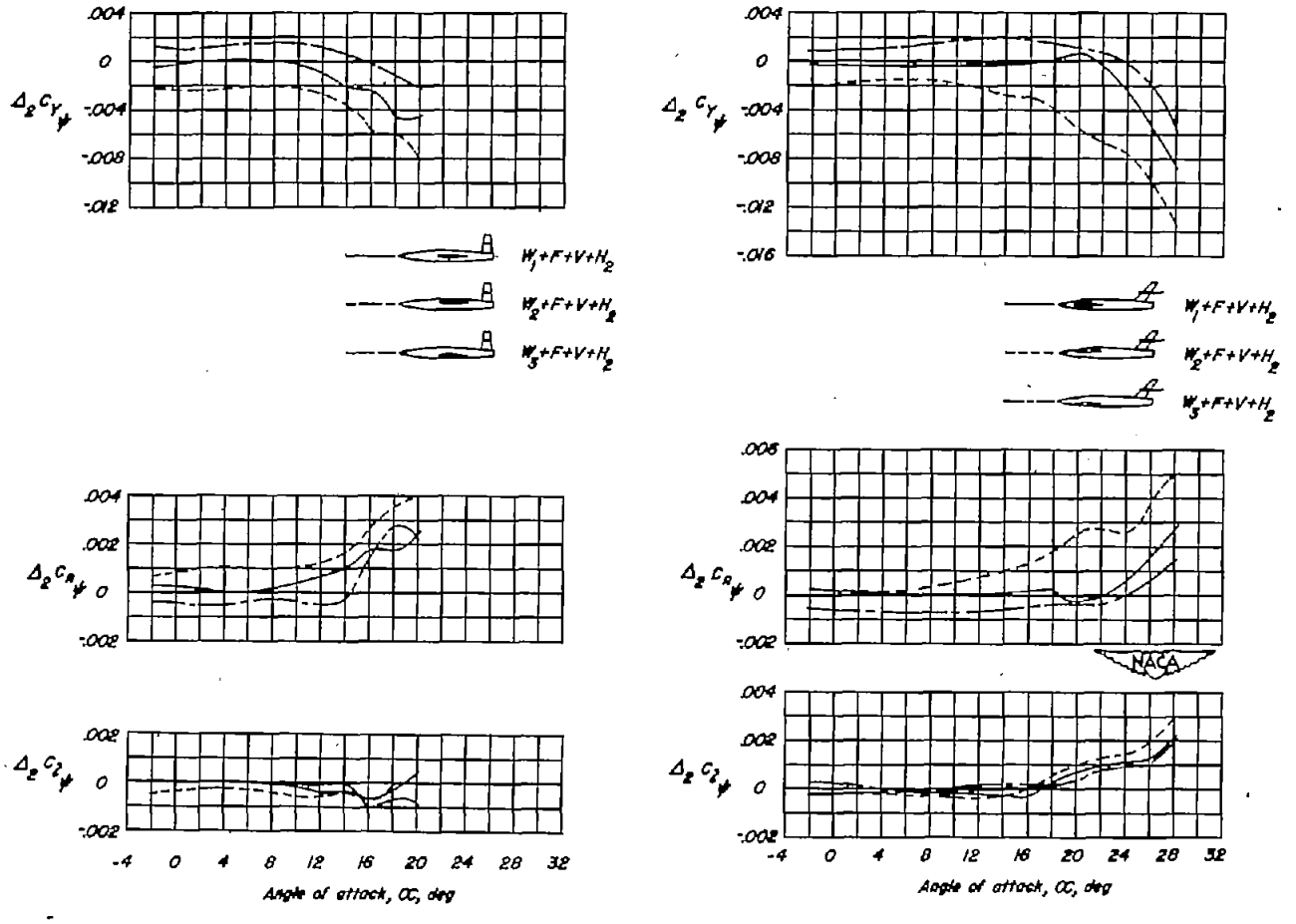

(a) $\Lambda = 0^\circ$.

(b) $\Lambda = 45^\circ$.

Figure 26.- Effects of wing position on the increments caused by wing-fuselage interference on the vertical tail contributions $\Delta_2 C_{Y_\psi}$, $\Delta_2 C_{n_\psi}$, and $\Delta_2 C_{l_\psi}$. High horizontal tail on.

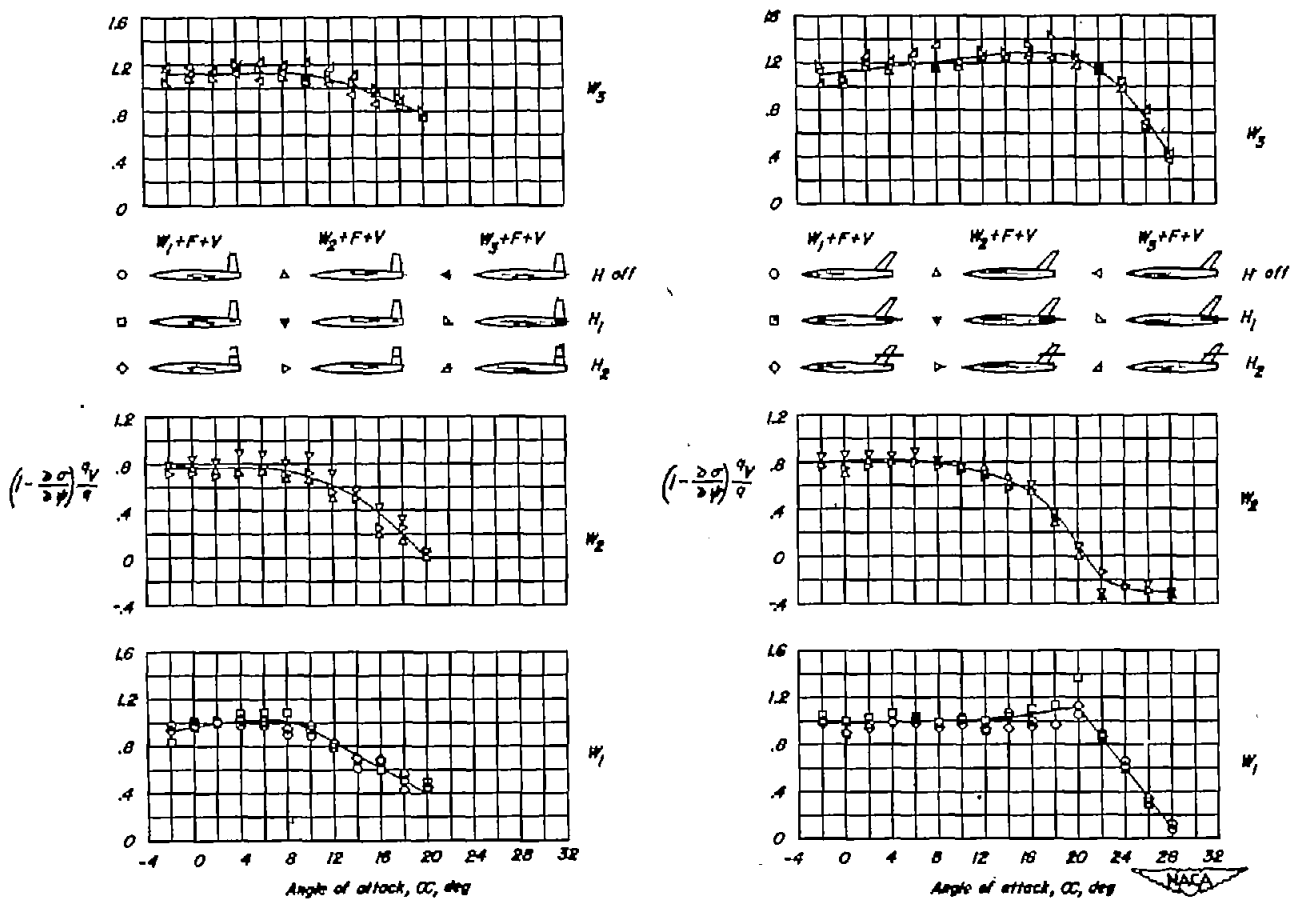

(a) $\Lambda = 0^{\circ}$.

(b) $\Lambda = 45^{\circ}$.

Figure 27.- Variation with angle of attack of the vertical-tail efficiency factor $\left(1 - \frac{\partial\sigma}{\partial\psi}\right)\frac{q_V}{q}$ for several wing and horizontal-tail heights obtained by equations (13) and (14).

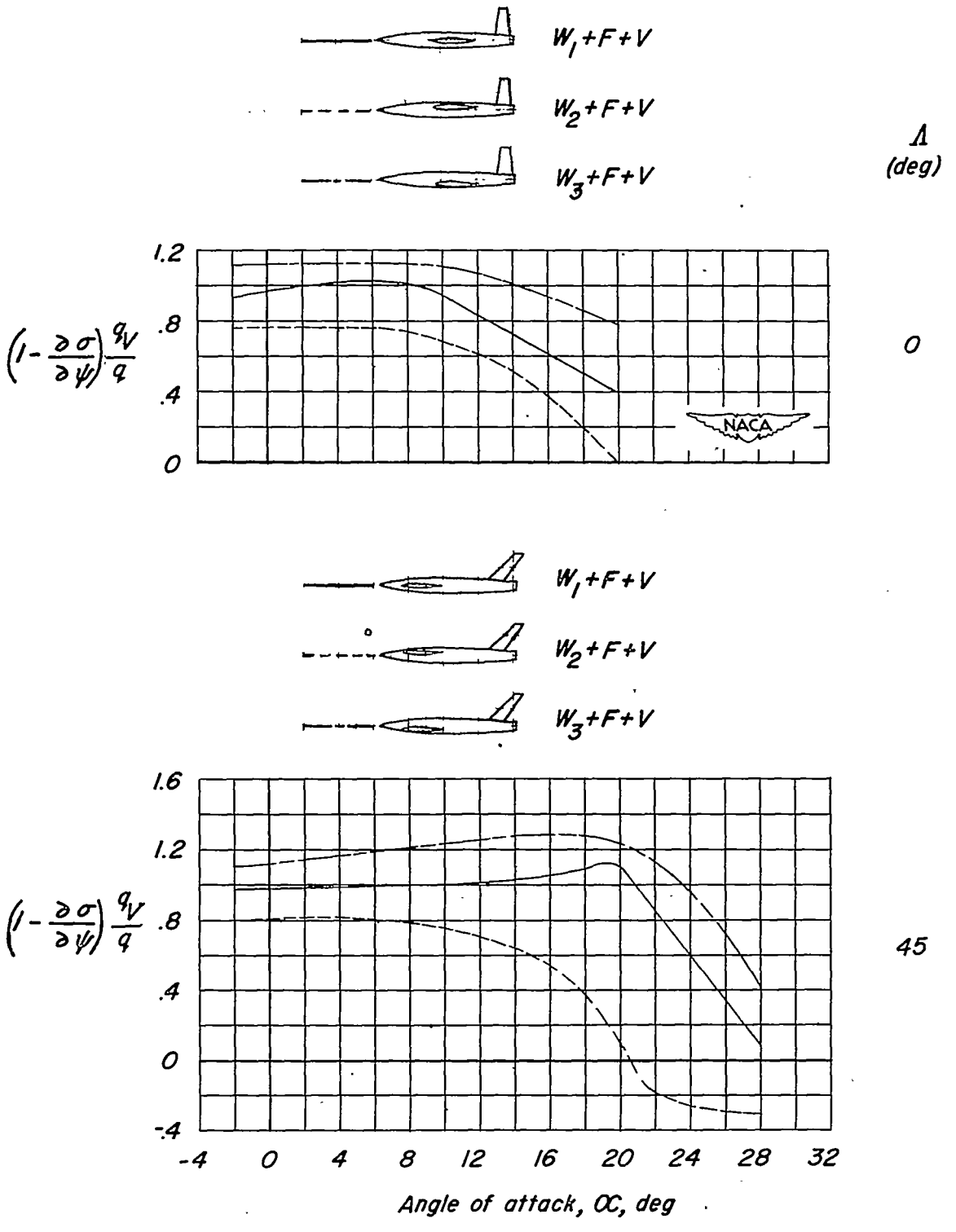

Figure 28.- Effects of wing position on the variation of the average efficiency factor (fig. 27) with angle of attack for the unswept and 45° sweptback configurations.

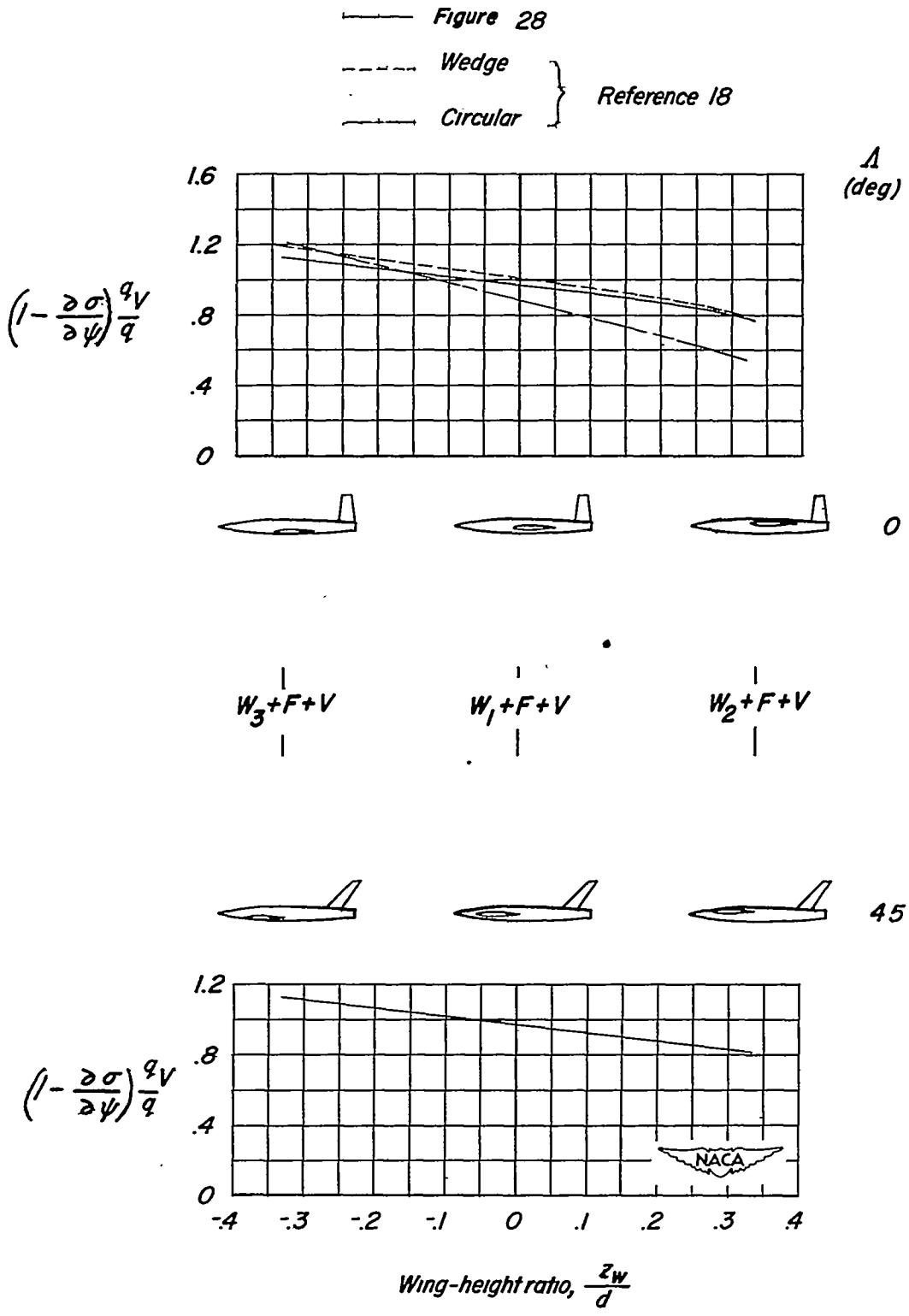

Figure 29.- Variation of the average efficiency factor with wing-height ratio. $\alpha = 0^{\circ}$.

NACA-Langley - 10-23-51 - 1000